Chapter

Super-Resolution Radiation Biology: From Bio-Dosimetry towards Nano-Studies of DNA Repair Mechanisms

Jin-Ho Lee and Michael Hausmann

Abstract

Past efforts in radiobiology, radio-biophysics, epidemiology and clinical research strongly contributed to the current understanding of ionizing radiation effects on biological materials like cells and tissues. It is well accepted that the most dangerous, radiation induced damages of DNA in the cell nucleus are double strand breaks, as their false rearrangements cause dysfunction and tumor cell proliferation. Therefore, cells have developed highly efficient and adapted ways to repair lesions of the DNA double strand. To better understand the mechanisms behind DNA strand repair, a variety of fluorescence microscopy based approaches are routinely used to study radiation responses at the organ, tissue and cellular level. Meanwhile, novel super-resolution fluorescence microscopy techniques have rapidly evolved and become powerful tools to study biological structures and bio-molecular (re-) arrangements at the nano-scale. In fact, recent investigations have increasingly demonstrated how super-resolution microscopy can be applied to the analysis of radiation damage induced chromatin arrangements and DNA repair protein recruitment in order to elucidate how spatial organization of damage sites and repair proteins contribute to the control of repair processes. In this chapter, we would like to start with some fundamental aspects of ionizing radiation, their impact on biological materials, and some standard radiobiology assays. We conclude by introducing the concept behind super-resolution radiobiology using single molecule localization microscopy (SMLM) and present promising results from recent studies that show an organized architecture of damage sites and their environment. Persistent homologies of repair clusters indicate a correlation between repair cluster topology and repair pathway at a given damage locus. This overview over recent investigations may motivate radiobiologists to consider chromatin architecture and spatial repair protein organization for the understanding of DNA repair processes.

Keywords: ionizing radiation, DNA damage, DNA repair, super-resolution localization microscopy, chromatin nano-architecture, spatial repair protein organization, molecular cluster analysis, molecular topologies

1. Introduction

Past efforts in epidemiological (nuclear power industry, atomic bomb explosions, nuclear reactor accidents, etc.) and clinical (diagnostic imaging, radiation

oncology, radiation therapy planning etc.) research strongly contributed to the current understanding of ionizing radiation effects on human organs, tissues, and cells [1, 2]. In principle radiation biology is based on effects of instantaneous (10^{-18} s) [3], stochastic damaging interactions of ionizing radiation with cells, a main target being the genetic material, i.e. chromatin in the cell nucleus [4]. In this context, radio-sensitivity and radio-resistance as opposing terms describe the extent of individual cellular susceptibility or 'response' upon radiation exposure which are highly dependent on physical (e.g., radiation type, dose, dose rate, etc.), chemical (e.g., hydroxyl radicals, etc.) and biological (e.g., developmental and proliferative state of the affected cell type) factors. As the overall organismal radiation response results from the entirety of all individual radiation responses on the single cell level, deeper understanding of the underlying, complex molecular mechanisms and dynamics of radiation induced DNA damaging and repair on the cellular level is highly relevant for fundamental and applied radiation biology (for review see [1, 2, 5]).

Hence, cytometric analyses based on fluorescence microscopy have become the method of choice to study damaging effects of ionizing radiation and DNA repair. This has contributed a lot to today's knowledge. However, conventional fluorescence microscopy is limited to average lateral resolutions around 200 nm laterally and 600 nm axially [6] and thus is limited to the bulk analysis of molecular cellular processes and structures. In parallel, super-resolution fluorescence microscopy techniques have rapidly evolved during the last few decades and turned out to be powerful tools to study cellular structures and molecular architectures on the nanoscale (for review see [6–8]). Methods based on stochastic reversible photobleaching [9–15] of single molecules called Single Molecule Localization Microscopy (SMLM) [16] reach effective resolutions down to 10 nm and have become popular among modern super-resolution imaging techniques as their realization is highly practical and straightforward using established specimen preparation methods of standard fluorescence microcopy [17]. As such resolutions allow the detection of single molecules, such as nucleosomes [18], proteins [19, 20], receptors and junction proteins [21, 22], or even single chromatin loops [23] etc., super-resolution microscopy opens new avenues for the research of radiation induced damaging and repair processes [5, 24].

With this article, we attempt to introduce the novel SMLM approach to radiation biophysics and radiation biology. We start with a brief summary on the basics of ionizing radiation, induction of DNA damage and damage repair mechanisms, to follow up with some standard radiobiology analysis methods. We further provide an overview of the working principles of selected sub-diffraction microscopy techniques with a focus on SMLM. Finally, the successful application of localization microscopy in radiation biology research is demonstrated along examples of current works.

2. Effects of ionizing radiation on cells and cell nuclei

Ionizing radiation penetrates through material and deposits enough energy to ionize molecules or atoms by liberating electrons. The effects of ionizing radiation on biological materials are highly dependent on the dose, the dose rate and type of radiation. In living cells, ionizing radiation hits all kinds of biomolecules, such as desoxyribonuleic acids (DNAs), aminoacids (proteins), lipids (membranes), carbohydrates, etc. However, most harmful consequences to living organisms show damages inflicted to their genomic DNA, especially in the form of DNA double-strand breaks (DSBs) [25, 26]. Especially follow-up effects of false strand repair may lead to significant dysfunctional development as for instance tumor genesis.

2.1 Ionizing radiation

Ionizing radiation (IR) includes all high energy/speed (> 1% speed of light) ions (e.g. carbon ions), atom nuclei (e.g. alpha particles), subatomic particles (e.g. beta particles, protons or neutrons) and high-energy electromagnetic waves (e.g. high energy ultraviolet (UV) rays, X-rays and gamma rays), that carry enough energy to directly or indirectly ionize atoms or molecules by liberating electrons from them, and to break molecular bonds [27].

The most common types of ionizing radiation occurring under environmental circumstances are caused by radioactive decay and can be divided into three groups: alpha, beta and gamma radiation [27]. Alpha radiation is made up of particles comprising two protons and two neutrons (helium nucleus) that carry energies in the range of up to several MeV. Due to its large particle size, alpha radiation has the lowest penetration depth through biological materials and the highest energy deposition per distance traveled. Beta particles are made up of electrons or positrons, thus exerting higher penetration depths and lower energy depositions compared to alpha particles. Gamma rays are high energy electromagnetic waves that exhibit the highest penetration and compared to particles, lowest energy deposition per track unit in biomaterials among these three types of IR. Due to the dispersed and low energy deposition in tissue, gamma and beta radiation are often referred to as low linear energy transfer (LET) radiation, whereas alpha particles belong to high LET radiation [27].

For clinical diagnosis and therapy in radiology or radiation oncology [28, 29], typically artificial radiation sources are applied, as for instance to produce X-rays in the energy range of keV to MeV, electrons and positrons, protons, and heavy ions (carbon or nitrogen). Like alpha particle, protons and heavy ions belong to high LET radiation. The advantage of protons and especially heavy ions is based on the characteristic absorbance with a Bragg peak at the end of the particle track where most of the particle energy is deposited. This energy positioning peak can exactly be localized in the tumor volume so that intact cells and tissues in the tumor surroundings are excluded from radiation damaging [30].

2.2 Dose measures

The absorbed dose D of ionizing radiation is quantified by the amount of energy deposited per unit mass of the penetrated material and is measured in units of Joule per kilogram (J/kg) or Gray (Gy) [27]. It describes an universal energy absorption for all types of ionizing radiation and is most commonly used in radio-physical research, whereas a radiation type specific dose also called the equivalent dose H calculated by multiplication with a weighting factor W_R (e.g. $W_R = 1$ for gamma radiation and $W_R = 20$ for alpha radiation) is often used in radio-biology, radio-medicine, or radiation protection and safety. The equivalent dose can be further weighted by a tissue weighting factor W_T to result in the effective dose E, which describes radiobiological effects considering the used radiation type and the tissue/organ of interest. Both, the equivalent dose and effective dose are quantified in units of Sievert (Sv) and do not represent physically measurable quantities but rather a value based on clinical and epidemiological outcome that is typically used in radiation safety [31].

2.3 Damages of DNA induced by ionizing radiation

Among all kinds of ionizing radiation induced biological effects, damages to chromatin especially the DNA molecules in the nucleus of cells are thought to be the

most severe with respect to cellular survival and carcinogenesis [2, 5, 32, 33]. DNA base oxidation, single strand breaks (SSBs) and double strand breaks (DSBs) are the most common ionizing radiation induced damages to the DNA molecule, that affect genome integrity and DNA biochemistry [34].

DSBs of DNA belong to the most complex and severe types of DNA damages as they directly affect genome integrity and the way of cellular survival [35–37]. Single strand breaks (SSBs) induced by ionizing radiation and base damages occur more frequently than double strand breaks [34]. It can be estimated to about 40 DSBs/Gy and about 1,000 SSBs/Gy. SSBs are less severe to genome integrity as an intact template strand is still available for complementarity-aided, error-free repair of the lesion. But DSBs are also simply formed by two or more opposing SSBs in close proximity or combinations of different DNA damage types [26].

Induction of DSBs in native chromatin is rapidly followed up by phosphorylation of nearby histones of the H2A variant H2AX at serine residues at position 139 [38]. This results in the generation of plenty γH2AX molecules around a DSB damage site, where about 2 Mbp of DNA are usually phosphorylated [39]. This leads to the formation of focus structures of sizes in the range of micrometers, which can be visualized under a fluorescence microscope [40]. These phosphorylated histones serve as signal and anchor points for many downstream recruited proteins of certain DNA damage response and repair machineries [41]. As the number of γH2AX foci is quantitative for DNA damage, counting of specifically labeled foci has been established as a measure for dose-efficiency and correlated to cell survival [42].

Single ionizing radiation induced DNA lesions can be caused by direct or indirect hits [43]. Ionizing radiation penetrating through a cell nucleus can hit and ionize atoms in a DNA molecule itself with a certain probability. However, the most prominent primary reaction underlying all ionizing radiation induced DNA damages is the radiolysis mediated formation of reactive oxygen species (ROS), e.g. •OH radicals, O2•- radicals and H2O2, which can further inflict reducing damage and thus lesion to the DNA [44]. Ionizing radiation, especially high LET radiation, is known for its property to efficiently induce highly complex damages to DNA. Such complex DNA damage sites composed of multiple lesions in close proximity on both strands are also termed locally multiple damage sites (LMDS) [45].

3. DNA double strand break repair mechanisms

Living organisms developed highly efficient and customized ways to repair the severe damages inflicted to their genome. The DNA DSB sites are rapidly (within seconds to minutes) recognized and marked by proteins of an initial response, which serve as signals and docking sites for more specialized proteins of DNA repair pathways. The fate of repair type depends on the concerted presence of pathway specific damage response proteins [1, 2, 46–48]. The main two ways by which cells respond to DNA double-strand breaks are non-homologous end joining (NHEJ; also called canonical NHEJ = cNHEJ) and homologous recombination (HR). NHEJ mediated DSB repair is fast and can be error-prone, but it can be flexibly performed throughout all cell cycle phases. HR works error-free, but is mostly restricted to late S and G2 phases as a homologous sister chromatid is required as a repair template [49–52]. Recent data, however, have suggested that active genes may employ HR also in G1 phase, by utilizing the nascent RNA as a template for precise repair (reviewed in [53]). As the DNA-end resection is inhibited in G1 cells, an alternative model with cNHEJ taking the advantage of the same principle (RNA-templated repair) has also been proposed. Interestingly, DNA repair by HR is preferred in lower eukaryotic life forms, whereas NHEJ is predominantly observed

in mammalian organisms. Alternative low abundant DSB repair pathways are the alternative end joining pathways (a-NHEJ; also called back-up EJ), micro-homology mediated EJ (MMEJ) and single strand annealing (SSA). One main difference between all DSB repair mechanisms is the extent of initial DNA end-resection at the damage site [26, 54–59]. The DNA damage response (DDR) against DSBs is subject to intensive radiobiological investigation and fluorescence microscopy of in situ DSB repair proteins serves as state of the art biological dosimetry.

3.1 The initial response

After the induction of a DSB, damage response proteins are rapidly recruited and accurately determine the fate of the DSB towards a repair pathway that best deals with the damage site in a certain genomic and cellular context. The chromatin remodeling p53-binding protein (53BP1) protects the break site from extensive end resection [60], thereby promoting repair by non-homologous end joining [61], whereas BRCA1 facilitates extensive end resection for repair by homologous recombination [52, 62].

3.2 Non-homologous end joining

The NHEJ repair pathway is initiated with binding of the Ku70-Ku80 heterodimer complex to the DNA ends of the DSB site, which serves as a linkage between damage site and further damage response proteins [61, 63]. In a second step, DNA-dependent protein kinase catalytic subunit (DNA-PKcs) is recruited to the Ku complex forming the DNA-PK complex. On-going recruitment of X-ray complex (XRCC4)/DNA Ligase IV (X4LIG4) complex and XLF to the DNA-PK complex forms the core NHEJ complex [64]. DNA-PKcs sterically protects the break site for repair and phosphorylates other repair proteins [65, 66] and H2AX [41]. Furthermore, DNA-PK auto-phosphorylation results in a conformational change of the core complex, thereby enabling DNA end processing by nucleases and dissociation of the DNA-PKcs subunit [67, 68]. Finally, ligation of the DNA ends is mediated by the X-ray complex (XRCC4)/DNA Ligase IV (X4LIG4) complex and XLF [69–71]. Artemis endonuclease [72, 73], polynucleotide kinase (PNK) [74], DNA polymerase (pol) μ and λ can be additionally involved in NHEJ repair depending on the chemical properties of the DNA damage site [75].

3.3 Homologous recombination

To initiate repair by HR, the free damaged DNA ends at the DSB site must be sensed and bound by a protein complex comprised of MRE11, RAD50 and NBS1 (MRN complex) [76]. Next, the protein kinase Ataxia Telangiectasia Mutated (ATM) [77] is recruited to the MRN complex at the damage site [78], which auto-phosphorylates and phosphorylates components of the neighboring chromatin. Most prominent phosphorylations are those of the histone variant H2AX (γH2AX), one of the earliest and a very sensitive marker of cellular response to DSBs [38]. End resection is initiated by the single-strand endonuclease and exonuclease activity of the Mre11 protein [52, 79] of the MRN complex. RAD50 further stimulates Mre11 nuclease activity and Nbs1 interacts with CtIP [80], another protein that is essential for the initiation of MRN complex mediated end resection [81]. Exonuclease 1 (Exo1) and Dna1/BLM are recruited by CtIP to continue end resection [82–84] until it gets attenuated by RPA coating of resected ssDNA ends [85]. BRCA2 in combination with BRCA1 and PALB2 dismantles the ssDNA ends from RPA coats enabling binding and forming of the RAD51 nucleoprotein filament, which stimulates

homology search and strand invasion [86]. Sister chromatid strand recombination via Holiday junctions is further facilitated by RAD54A and its paralog RAD54B [87, 88], finally resulting in conservative repair of the DNA lesion.

3.4 Alternative repair pathways

a-NHEJ or b-NHEJ has been described in slightly different ways which are not well distinguished [56–58]. Mostly, in the presence of short micro-homologies (>4 bp) after CtIP-MRN mediated end resection, repair via an alternative end joining (MMEJ) can take place [89]. This is initiated by Poly(ADP-ribose) polymerase 1 (PARP1) and followed up by DNA polymerase θ (pol θ) mediated strand extension starting at the paired micro-homology site. Ligase1 and Ligase2 are supposed to perform the final ligation of DNA ends [90, 91].

When the damage site is flanked by larger regions with non-allelic sequence homologies, repair by single-strand annealing is also possible. The absence of Ku proteins and even more extensive end resection to expose the homologous regions as single strands are necessary for SSA repair [92]. Again, RAP binding to the resected ends promotes RAD52 mediated annealing of homologous regions. Nuclease XPF-ERCC1 trims the remaining non-homologous overhangs and DNA Ligase 1 connects the DNA ends [93].

Several studies indicate, that damaged genomic Alu elements use micro-homologies for single-strand annealing, thereby often leading to translocations [94, 95]. Such nonconventional damage repair processes might explain a significant portion of the observed deletion events associated with malignancies [59]. In fact, in vitro model systems could already demonstrate Alu mediate non-allelic homology dependent DSB repair [96].

4. Radio-sensitivity and biological dosimetry

Radio-sensitivity can be assessed on different scales ranging from whole organs and tissues over single cells to molecular markers and mechanisms. Based on clinical and experimental findings on DNA damage induction and response mechanisms, the dose effect of ionizing radiation on biological material is commonly described with a linear-quadratic model [97, 98]. At low dose ranges (below 1 Gy), radiation damages are supposed to linearly increase with the applied dose, whereas at higher doses the probability for multiple hits increases and complex DNA damage spots dominate.

In this chapter, we summarize some established methods to study cellular and molecular effects of ionizing radiation. In the past, sophisticated assays were developed to detect and quantify radiation induced damages to the cell and nuclear DNA ranging from techniques to assess overall cell survivability, large-scale chromosomal damages and rearrangements over sensitive detection of DNA break sites to modern state of the art technologies that can visualize the formation of damage foci in situ with the help of suitable biomarkers.

a. Colony forming assays (CFAs) based on clonogenic survival (also called clonogenic assay) (see [99] and citations therin) as a method to quantify cell survival after radiation exposure was firstly described by Puck and Marcus in 1956 [100]. CFAs measure the ability of cells to divide after treatment with agents that impair cellular reproduction, e.g. radiation (**Figure 1**). Since then, colony forming assays were improved for many different cell types and are widely used as a “gold standard” in radiobiological studies. In practice, irradiated

cells are plated at higher dilutions so that single cells are well separated. Upon incubation colonies form each originating from a single cell. Thereby, colonies comprising 50 cells or more are considered for estimating the survival fraction. Treatments such as exposure to ionizing radiation damages the reproductive survivability of cells and thus results in a lower number of colony formation events at the same number of plated cells [103].

b. A fraction of ionizing radiation induced DNA double strand breaks results in heavy genomic rearrangements that can be detected on metaphase chromosomes. False rearrangements of multiple centromeric regions between chromosomes can lead to dicentric, acentric, centric ring conformations [104, 105] that can be visualized under a conventional fluorescence microscope (**Figure 2a**). The good reproducibility and comparability lets the so called dicentric assay stand among the gold standards of biological dosimetry [106]. Nowadays dicentric assays are further developed towards biological dosimetry in the low dose range (< 500 mGy).

c. The micronucleus test is a method to assess and detect chromosomal breakages in interphase nuclei developed by Schmid et al. in 1975 [107]. Radiation damage can result in major chromosomal aberrations and loss on the centromeric region by wrong rearrangement of DNA double strand breaks (**Figure 2a**). These heavily damaged acentric chromosomes can form separated globular structures outside the main nucleus in interphase. As micronucleus formation can be readily detected in interphase nuclei, analysis can be performed much faster and serves as an efficient alternative for the analysis of instable chromosome aberrations [108].

d. In 1984, Ostling and Johanson published a micro-electrophoresis technique that could visualize DNA damages in single cells [109]. First, cells are embedded in agarose and lysed with non-ionic detergents under high salt concentrations, so that only nucleoids (supercoiled DNA loops attached to the nuclear matrix) remain. Ionizing radiation-induced breaks relax and locally unwind the supercoiled DNA structure, thereby partly linearizing the strand at the break site. When voltage is applied linearized DNA segments (SSB) protrude from the nucleoid and migrate faster towards the anode while the nucleoid core remains assembled. The nucleoid and its tail resemble a comet, when stained with 4′,6-diamidino-2-phenylindole (DAPI) or other quantitative DNA fluorescence dyes and visualized under the fluorescence microscope, thus leading to the term 'comet assay' [110, 111]. Alkaline variations of the comet assay

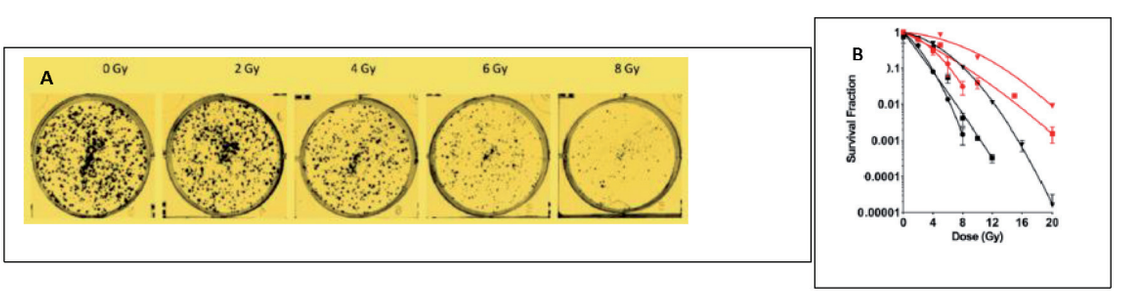

Figure 1.
(A) Example of colony formation after cell exposure to different doses of X-ray irradiation. (B) Typical survival curves for cell colonies after irradiation with different types of photon and particle radiation. Linear-quadratic cell survival curves are fitted and can be used to calculate the relative biological effectiveness. Note: These figures are modified and were originally published under CC BY license in [101, 102].

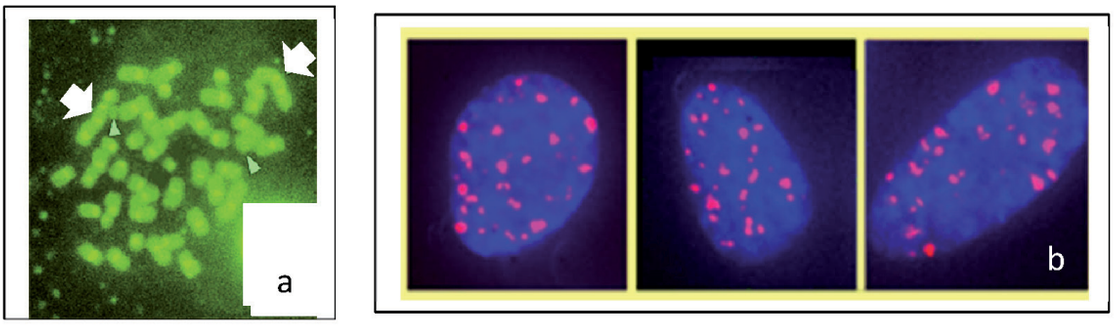

Figure 2.
(a) Example of a lymphocyte metaphase plate with centromeres highlighted by FISH. The cells were irradiated with 3 Gy X-rays. The big arrows show two dicentric chromosomes. The small arrow heads label the corresponding acentric fragments. (b) Typical examples of fibroblast nuclei (stained with a specific DNA dye) with γH2AX foci after exposure to high dose irradiation. The foci are labeled by specific antibodies.

[110] were introduced, that can detect DNA damages over an extended dose range (0.25 Gy to 2 Gy) than under neutral pH conditions (1 Gy - 3 Gy) [111]. Modern approaches extend the method by automatization of experimental procedures and image analysis [112–114], thereby enabling statistically robust high-throughput detection of DNA damages for potential clinical applications.

e. DNA damage response proteins like γH2AX, 53BP1, RAD51 etc. accumulate at initial damage sites and rapidly form foci-like structures in the nucleus (see for example **Figure 2b**). Antibody staining and fluorescence microscopy of such damage response proteins is an established tool to visualize and quantify DNA damage repair foci at single cell resolution. One advantage of this technique is the ability to assess molecular dynamics of DNA damage repair by visual observation of foci formation at different time points after irradiation.

5. Super-resolution radiation biology

Fluorescence microscopy of potent marker labels is a powerful analysis tool to assess cellular effects of ionizing radiation on the single cell level by optical examination. Due to past efforts, a myriad of fluorescent probes exists for the molecular labeling of almost any known biological target structure (e.g. specific antibodies against γH2AX, 53BP1, MRE11, RAD51 or other repair proteins as well as against heterochromatin or euchromatin etc.). This opens the door to analyze molecular mechanisms underlying fundamental biological functions by optical investigation, e.g. DNA damage response and repair dynamics upon ionizing radiation exposure [1, 2, 5].

5.1 Super-resolution microscopy

A variety of novel super-resolution microscopy techniques were invented in the last few decades [115]. With the help of novel super-resolution microscopy techniques, the molecular effects of ionizing radiation in single cells can be studied on the nanoscale. Nano-labeled molecular structures can be resolved in biological specimens down to a precision of 10 nm (1/50 of the wavelength of visible light), which is in the range of single nucleosomes, antibodies, receptors, etc. (see for example [20, 21]).

In order to improve the resolution in light microscopy, a prerequisite is to circumvent the diffraction limit of light, a physical phenomenon firstly described by

Ernst Karl Abbe and John William Strutt, 3rd Baron Rayleigh, during the late 19th and early 20th century [115]. In diffraction limited fluorescence/light microscopy, the Abbe or Rayleigh criterion (**Figure 3**) is commonly used to define a resolution measure describing the minimal distance D between two point-like light sources with wavelength λ that can be resolved:

$$D = 0.61\,\lambda / NA \tag{1}$$

Therein λ is the wavelength and NA the Numerical Aperture of the objective lens (NA = n sin(α/2); n = refraction index; α = lens aperture angle). Conventional fluorescence microscopy techniques that use objective lenses with high numerical aperture NA (≥ 1.4) are available today. In confocal laser scanning microscopes, they typically achieve resolutions down to 200 nm in lateral and 600 nm in axial direction. However, modern super-resolution microscopy using the same objective lenses circumvent this physical limit by sophisticated interaction with fluorescence signals so that they can visualize biological specimen down to resolutions in the order of 10 nm, which is in the range of single nucleosomes, antibodies, receptors, etc. [16].

A complete overview of super-resolution microscopy techniques is beyond the aim of this article. However, we want to mention some meanwhile very well established ones:

Sophisticated near-field super-resolution methods, e.g. total internal reflection fluorescence (TIRF) microscopy (TIRFM) [118, 119] or near-field scanning optical microscopy (SNOM, NSOM) [120, 121], belong to the first techniques breaking the diffraction limit by novel techniques working in the optical near field of fine crystal tips probing the specimen without an microscope objective lens. Unfortunately, near-field techniques are technically restricted to the visualization of surfaces of cells, membranes or isolated organelles [122–124].

More recently evolved far-field super-resolution fluorescence microscopy techniques use objective lenses available from establishes microscope manufactures and can be separated into two principle approaches. The first is based on the spatially modulated excitation of fluorophores, e.g. by point spread function engineering as in stimulated emission depletion (STED) [125] or by excitation through a series of illumination patterns as in structured illumination microscopy (SIM) [126]. A second group of super-resolution techniques is based on optical isolation of fluorescent molecules through switchable intensities [17] or intrinsic differences in spectral signatures [127]. The latter techniques often referred to as single molecule localization microscopy (SMLM) in general, can be practically implemented with customary microscope parts and standard objective lenses [16]. Spectral precision distance microscopy (SPDM) an early development of the 1990s [128] is the one and only localization microscopy method, that establishes optical isolation of molecular labels through constant differences in absorption and emission spectra of different fluorophores, that are applied in a combinatory labeling strategy [127, 129]. Most localization microscopy methods, however, rely on stochastic spectral modulations of single fluorophore molecules, such as photo-activated localization microscopy (PALM) [12], fluorescence PALM (FPALM) [13], stochastic optical reconstruction microscopy (STORM) [15, 130], direct STORM (dSTORM) [131], ground state depletion microscopy followed by individual molecule return (GSDIM) [132], SPDM with physically modifiable fluorophores ($SPDM_{phymod}$) [14, 17], etc. In the following chapters, we will describe single molecule localization microscopy in more details as being applied in radiation biophysics and we will provide examples indicating wide applications in nano-probing biomolecules and molecular mechanisms.

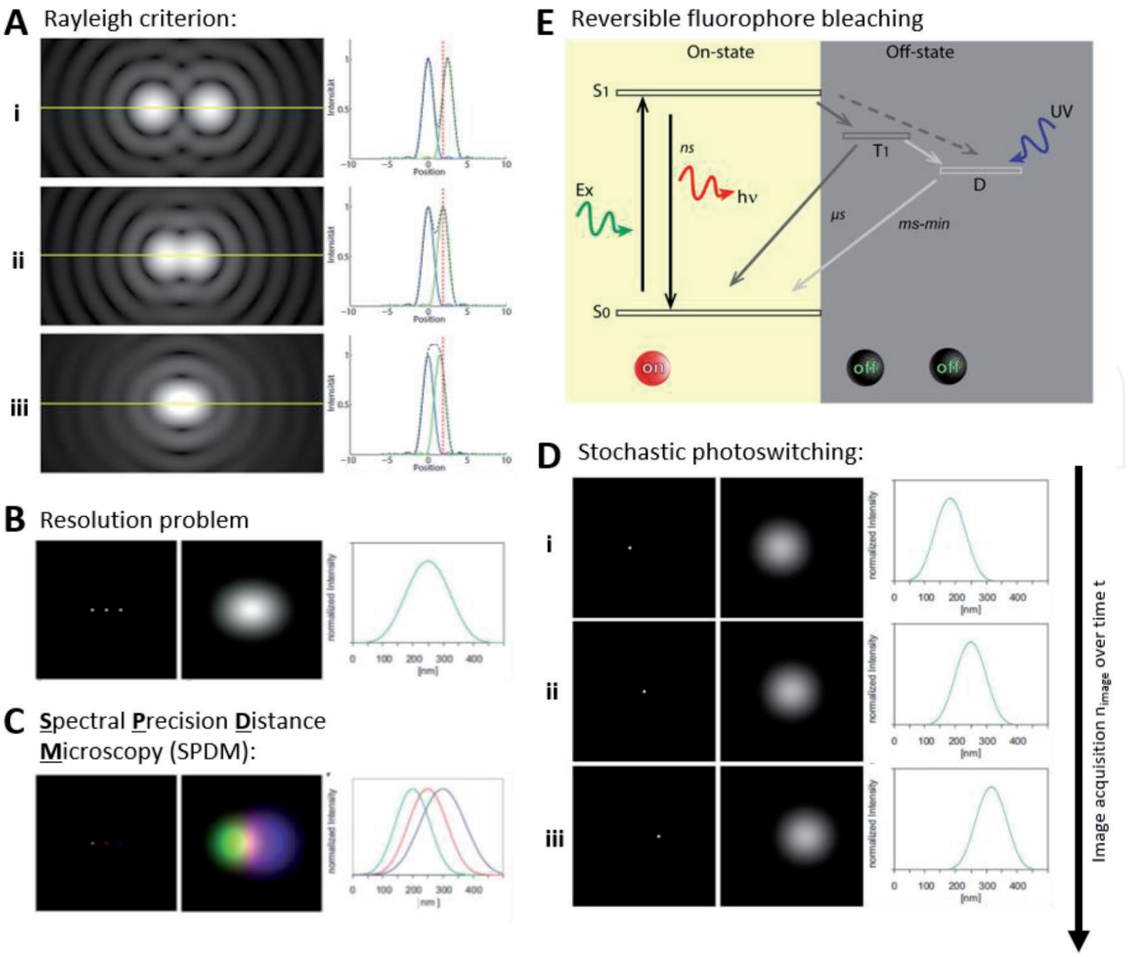

Figure 3.
Rayleigh criterion for the diffraction of two point-like light sources and single-molecule localization microscopy techniques to circumvent the diffraction limit. (A) The resolution limit of two adjacent point-like sources of light is defined by the distance between these two light points; the first intensity minimum of one light point overlaps with the main intensity maximum of the other light point. (B) The diffraction limited resolution of fluorescence microscopy illustrated by an example of three point-like signal sources within a distance below the resolvable range. (C) Working principle of SPDM by spectral isolation of labeling molecules. Here the spatial positions of three point-like fluorescent light sources can be separated by three different colors green, red and blue (from left to right). (D) Working principles of most single molecule localization microscopy methods rely on spectral modulation that switches most fluorophores into a dark state in a stochastic manner. Thereby, detection of only a sparse subpopulation of labels that are either totally isolated or lie apart at distances greater than the diffraction limit is possible. A series of acquisitions, each representing another stochastic sparse subpopulation of signals, can be summarized to result in a complete image below diffraction limit. (E) Minimal Jablonski diagram showing the electronic states and transitions involved in the intrinsic stochastic blinking of fluorophores. Note: These figures are modified and were originally published under CC BY license in [116, 117].

5.2 Single molecule localization microscopy for radiation biophysics

Single molecule localization microscopy is one the most popular super-resolution techniques, because it can be practically realized with standard optical setup and standard specimen preparation methods using commercially available fluorophore labels. Fundamental to all SMLM techniques is the stochastic sampling of signals. The intrinsic blinking nature of a variety of available fluorophores at excitation with high laser powers (in the range of several kW/cm^2), enables SMLM with conventional dyes like GFP / YFP, Alexa488, Alexa568, etc. [16, 17, 133].

Apart from conventional fluorescence, which is based on rapid, repetitive excitation (10–15 s) and red-shifted emission (10–9 s) between the ground state S_0 and excited singlet state S_1, fluorescent molecules additionally undergo inter-system crossing (ISC) [134] from S_1 to dark triplet states T_1 [135]. From there, fast

relaxation (10–3 s) to the original S_0 ground state enables re-entry to new cycles of normal fluorescence (**Figure 3E**, left). Further transition from the T_1 state into a second dark state D also occurs, which takes longer (ms to min) to recover to the ground state S_0 (**Figure 3E**, right) [116, 136]. This reversible photobleaching via the long lived dark state D results in a limited number of stochastically blinking fluorochromes at resolvable time scales that can be used in single molecule localization microscopy to determine sub-diffraction positions of single fluorescing molecules [133].

For image acquisition, a time series of raw diffraction limited images (several hundreds to a few thousand) from the same region of interest are registered and efficiently searched for blinking events under a user-defined intensity threshold to discriminate signals from background. Then, the intensity profile of each blinking event is fitted by a Gaussian curve and the barycenter point of the signal source is calculated. Notably, the localization precision of such a point merely depends on its intensity/background ratio [137].

A major advantage of SMLM approaches lies in the data format. The point matrix containing the lateral x and y coordinates of each localization signal allows all kinds of mathematical and statistical analyses (**Figure 4**). Most prominent are analyses based on Ripley's point-to-point distance information which can be used for the elucidation of signal densities, cluster formation, and spatial organization of labels [139]. Recently, novel mathematical approaches like persistent homology determinations were introduced to investigate topological similarities [138]. Computation of the coordinate matrix into an image with user-defined resolution and visual enhancements is then possible. If provided, multi-color analyses on the single molecule level can be performed to study more complex molecular mechanisms and dynamics.

5.3 Applications of single molecule localization microscopy in radiation biophysics and biological dosimetry

5.3.1 γH2AX clustering and chromatin arrangements at DNA damage sites

Phosphorylated histone variant γH2AX molecules at the site of DSBs and their accumulation into γH2AX-foci are well-established markers of DNA damage response and repair. Most recent studies performed SMLM of γH2AX specific antibodies in HeLa cells that were exposed to different doses of γ-radiation and fixed at different time points after radiation exposure [140]. Quantitative analysis resulted in a linear quadratic increase in measured γH2AX localization signal points and cluster numbers with increasing doses of radiation exposure (**Figure 5A**, **B**). With increasing repair time, the number of γH2AX clusters decreases; thereby successfully demonstrating repair dynamics and cell recovery by γH2AX-cluster relaxation on the molecular level. As dose responses and molecular dynamics for γH2AX clusters and raw γH2AX signal points well correlate with past observations, this study can serve as a benchmark standard for future super-resolution radiobiology experiments.

Similar studies indicated that the γH2AX cluster size remained constant during repair also at later times post irradiation, i.e., at later times only the number of clusters reduced. This typical size was about 400 nm in diameter after photon irradiation and nearly independent from dose or the cell types analyzed [140, 141]. For α-particle irradiation from radioactive decay [142], the γH2AX cluster size along the particle track was about 200–300 nm; this size could be also observed for γH2AX clusters induced by environmental stress as for instance the deficiency of folat during long time culturing [143].

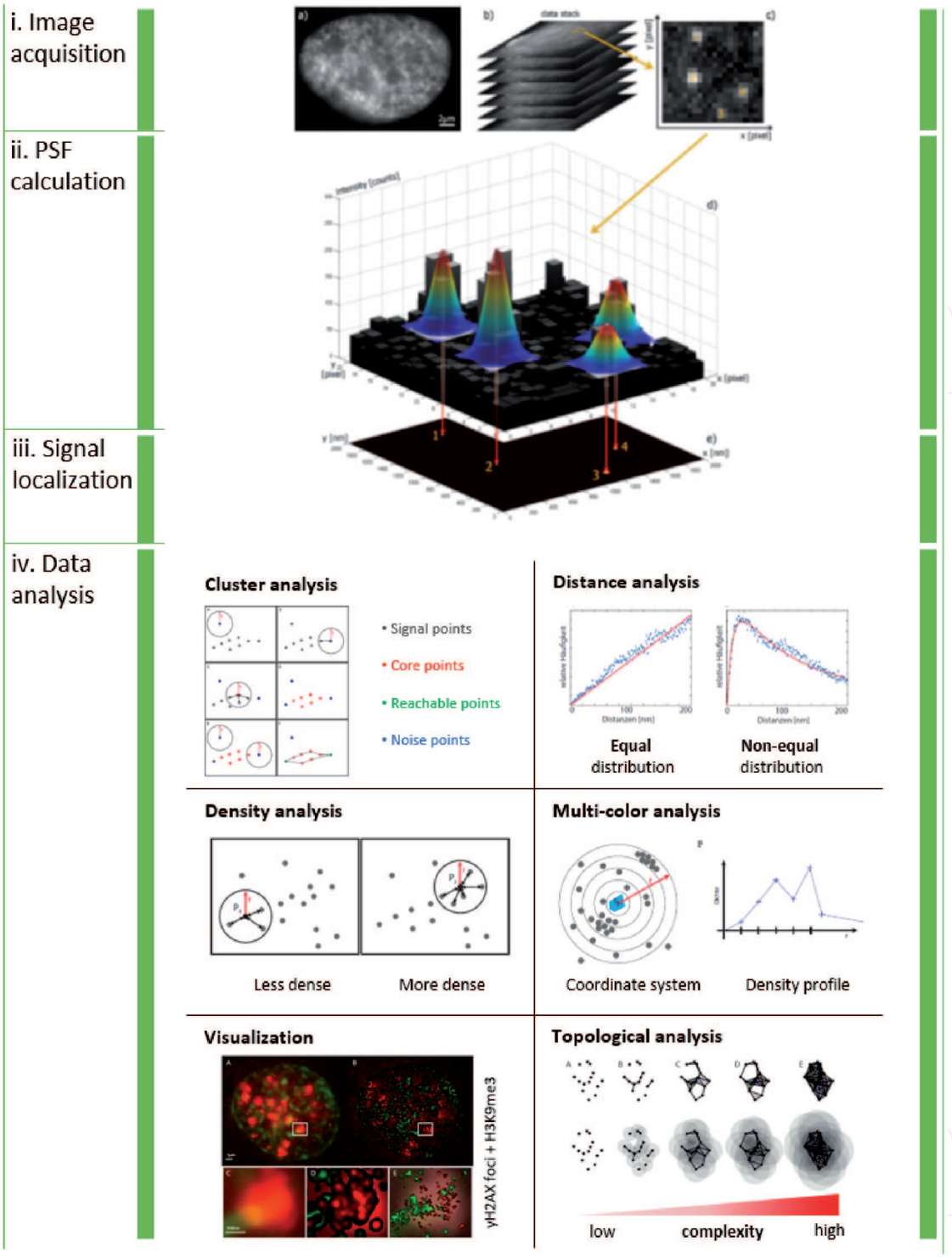

Figure 4.
General workflow of single molecule localization microscopy and data analysis. Serial images are acquired from the same region of interest (i). The point-spread function of each blinking event in each single image is gauss fitted to estimate the intensity maximum (ii), which represents the idealized lateral coordinates of the signal source (iii). The result is a data table containing the coordinates of all detected signal points. The matrix representation of data allows mathematical and stiatistical analysis of clustering, distance distributions, signal densities, multi-color signal distributions, enhanced visualization and topology (iv). Note: These figures are modified and were originally published under CC BY license in [16, 117, 138].

After exposure to photon radiation (different doses and energies) the SMLM analysis of heterochromatin around γH2AX clusters using specific antibodies against H3K9me3 methylation sites, revealed a fast relaxation of the chromatin and slower re-condensation after finishing the repair processes [144]. The degree of

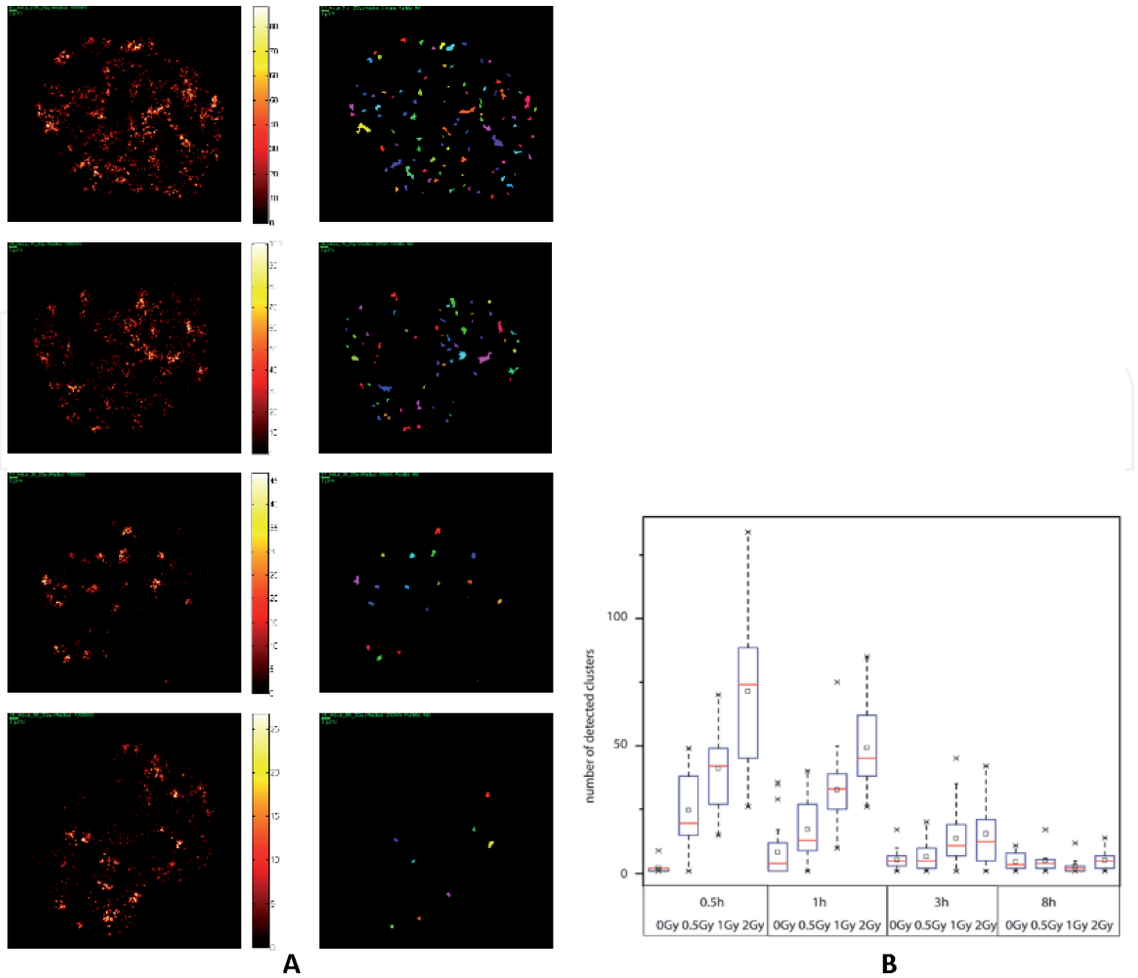

Figure 5.
(A) "Visualization of cluster formation from the SMLM image of cell nuclei after 2 Gy radiation exposure. Left column: *Density image obtained from the coordinate matrix and the next neighbor distance. The point intensity (see intensity scale bar) refers to the next neighbor frequency.* Right column: *Resulting clusters. The points belonging to a cluster are represented by a closed area (colored spots) and reflect nano-clusters within γ-H2AX foci.* Top > Bottom: *30 min, 1 h, 3 h, 8h post irradiation. (B) Numbers of γ-H2AX clusters per cell vs. dose and repair time. The boxplots show the mean cluster number per nucleus (small black square boxes), the median (red line), the lower and upper quantile (big box), and the value range within ± 2 standard deviations (dashed line). The black crosses refer to values that are differing more than 3 box lengths from the median." These figures together with the text of the relevant figure legend are reproduced from [140] with permission from the Royal Society of Chemistry.*

relaxation was independent of the dose which is in good relation to the equally sized γH2AX clusters [140, 141]. In contrast the euchromatin density increased during repair followed by a decrease after finishing the repair processes [144]. However, in total the chromatin showed an increasing clustering during repair followed by a reduction of clusters dependent on the energy of the damaging photons (unpublished). In general it can be assumed that DNA damaging by ionizing radiation does not only induce a reorganization of chromatin at the damaged sites but may also induce long range chromatin rearrangements for repair processes. Whether such chromatin rearrangements are random or directed to improve repair protein recruitment will be subject of future investigations.

5.3.2 Clustering of repair proteins at DNA damage sites

Beyond γH2AX cluster formation, foci and sub-foci clusters of repair proteins were investigated after photon or particle irradiation [141, 142, 145–147]. In the following, some typical examples are shown taken from ongoing projects:

1. 53BP1 foci were investigated in differently radio-resistant cell types, the moderately radio-resistant neonatal human dermal fibroblast cell line (NHDF) and highly radio-resistant U87 glioblastoma cell line. Specimens of both cell types were exposed to high-LET ^{15}N-ion radiation of doses of 1.3 Gy (in a 10° irradiation scheme) and 4.0 Gy (in a 90° irradiation scheme) at the particle irradiation facility of the Joint Institute for Nuclear Research, Dubna, Russia [145, 146].

   At given time points up to 24 h post irradiation, SMLM of fluorescently tagged 53BP1 molecules was performed and the coordinate data of each labeled molecule were quantitatively evaluated [137, 139, 140]. Clusters of these tags were determined as sub-units of repair foci (**Figure 6a**) and the formation and relaxation of these clusters revealed a higher ratio of 53BP1 proteins being recruited into clusters in NHDF cells (less radio-resistant) as compared to U87 cells (more radio-resistant) with different levels of distribution prior to DNA damage induction. This relation of 53BP1 inside and outside particle track clusters (**Figure 6b**) remained different for both cell types during the repair time observed. This could be seen as a measure of the "just-in-time" availability of 53BP1 proteins but did not reflect the absolute number of 53BP1 proteins available. The speed of cluster formation and relaxation differed for the two cell types (**Figure 6c**) indicating the recruitment of the existing proteins in the cell nucleus (higher in U87 cells) rather than a de novo production [147].
   A certain number of the clusters remained persistent, even longer than 24 h post irradiation (**Figure 6b**); thereby the number of these remaining clusters varied in each cell line. The heavily damaged cell nuclei maintained repair activity in order to process the complex damage patterns caused by high-LET ^{15}N-radiation. This long-standing repair activity of 53BP1 proteins was shown in both cell types and the behavior of the cells could causatively be linked to the cell-type specific radio-resistance.
   The dynamics and cluster formation of tagged 53BP1 molecules showed that these clusters were embedded within a random distribution of points. After irradiation, a fast formation of 53BP1 clusters was observed (**Figure 6c**). During the early repair time of about 30 min - 1 h after radiation exposure some clusters were dispersed while others persisted and the amount of randomly distributed proteins was growing. The latter clusters that were persistent did not disappear until the end of the repair period being studied (24 h).

2. Another study performed two-color SMLM of immunostained γH2AX and Mre11 proteins [141] and revealed significantly delayed foci formation by Mre11 compared to γH2AX. While γH2AX clusters are already established at 30 min after radiation exposure (**Figure 7**, left), Mre11 is still ubiquitously distributed in the nucleus. Mre11 cluster formation is maximal at around 180 min after irradiation with significant association to γH2AX clusters (**Figure 7**, right).

5.3.3 Topological similarities of repair clusters

The reason to apply topological analyses is to record properties of point patterns, which are invariant under certain deformations of the object. Mathematically these deformations correspond to continuous transformations of the topological space defined by the structures. Here we have considered two properties, the number of "components" (explained below), which are independent from each other in such sense that connections between points only exist within the respective components

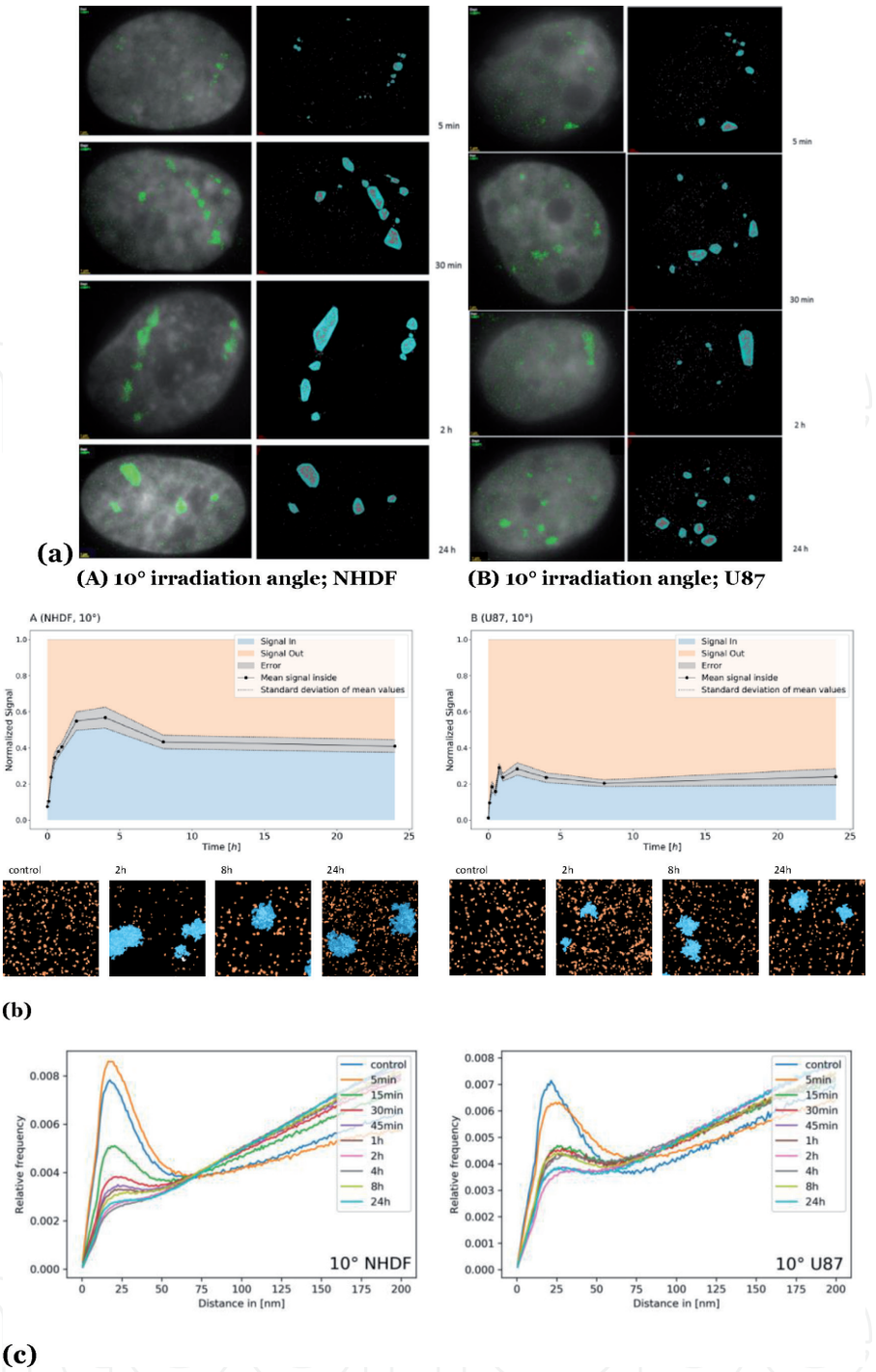

Figure 6.
(a) 2D density SMLM images of 53BP1 repair proteins. Typical examples are shown for fluorescently-labeled 53BP1 proteins in NHDF cells (a) and U87 cells (B) "after 1.3 Gy tangential ^{15}N-irradiation (10° angle between the ion beam and the cell layer). The time values indicate the period post irradiation when the samples were taken as aliquots of the same irradiated culture and fixed. For comparison, examples of non-irradiated control cells are presented. The left columns are merged images of SMLM data and wide-field images. In the right columns the SMLM images clusters and cluster areas are shown. The scale bars equal to 1 μm." (b) relative amounts of 53BP1 signals detected within (blue) and outside (orange) repair clusters. "Graphs: Mean values and margins given by the standard deviation are depicted in gray. The values are always normalized to the mean number of signals detected at a given time point. The data are presented for NHDF fibroblasts (A) and U87 cells (B) after 1.3 Gy tangential ^{15}N-irradiation (10° angle between the ion beam and the cell layer). Images: The pointillist images represent examples of sections of cell nuclei with labelling points inside (blue) and outside (orange) clusters at the given time points. The samples were taken as aliquots of the same culture at different time points (from 5 min to 24 hrs) after irradiation. For comparison, examples of non-irradiated control cells are presented (= 0 min)." (c) Ripley distance frequency analysis. The relative frequencies of pairwise distances are presented for the aliquots of the irradiated cell samples at different time points post irradiaton (color label of curves); (A) NHDF and (B) U87cells irradiated under 10° irradiation angle. Note: These figures are modified and the parts of the text written in "..." are reproduced from the original figures which were originally published under CC BY license in [146, 147].

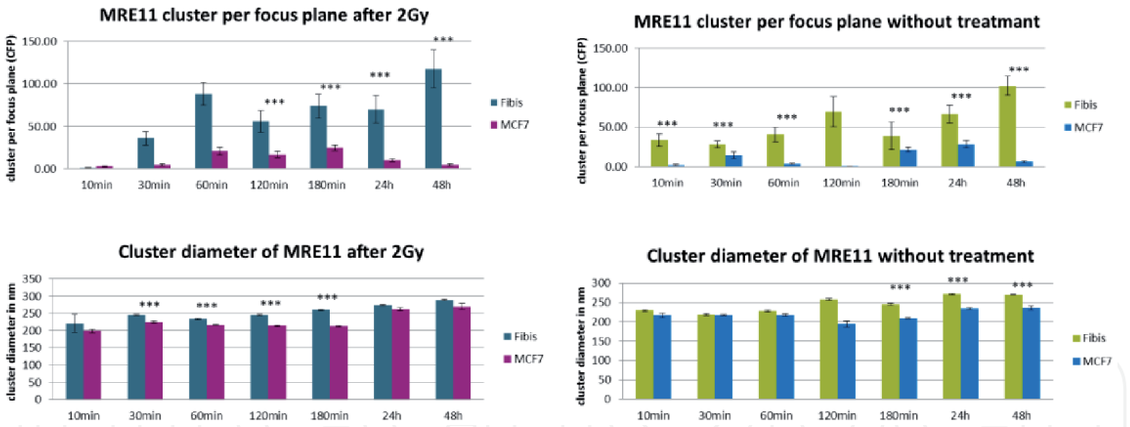

Figure 7.

*Overview of the results obtained from SMLM measurements. Left panels show the data obtained after radiation exposure for MCF-7 breast cancer cell nuclei ("MCF-7") in comparison to cell nuclei of CCD-1059SK fibroblasts ("Fibis"); right panels show the data obtained without radiation treatment, i.e., the natural occurrence of MRE11 clusters in these cells. The columns of each panel represent the mean values calculated from 20 nuclei each. The error bars on top of the column indicate the standard deviation. For each time step after the irradiation process, the data are given for cells exposed to 2 Gy ionizing radiation and for cells subjected to the same culturing procedure but not to radiation treatment. Level of significance between the corresponding values: *** = 0.1%. Note: These figures and their legends in "." are slightly modified and were originally published under CC BY license in [141].*

and the number of "holes" of the structures inside the components (explained below, **Figure 8a**). In algebraic topology, these properties are called the Betti numbers for zero and one -dimensional simplicial complexes [148].

SMLM images as for instance of γH2AX foci/clusters are point-sets for which components and holes can be defined. A geometric relationship among the points is defined by growing spheres of radius α around each of them. Whenever two spheres mutually embed each-other's center, these centers of the growing spheres are connected and the connected points belong to the same component. With increasing radii, the number of components is reducing. At the end of the procedure, a single component is remaining, the whole γH2AX cluster. For the definition of holes, a polygon is appropriate. Whenever the edges form a closed area, a hole is counted until another line closes a triangle separated from the original hole [147, 148].

The results are presented as "barcodes" to track the formation and disappearance of components and holes with increasing α (**Figure 8**, left panel). These barcodes offer easy comparison of different sets of barcodes and their similarity can be calculated by the Jaccard index [149]. The Jaccard index results is a value between 0 and 1, where 0 is equal to no overlap of two bars and 1 describes two identical bars. Barcodes of different dimensions are defined as similar, if the averages of the individual similarity indices fulfill the Jaccard index conditions of similarity. Importantly, topological comparisons are independent of the scale so that it is possible to compare variably large clusters.

The barcode transfers the examined structures into a form of visualization that is scale invariant. The formation and dissolution of small scaled complexes is recorded alongside the lifetime of large scaled complexes. Consequently, for γH2AX clusters, the barcodes contain bars representing components and holes in the nanometer but also in the micrometer scale ranges. In **Figure 8** (right panel) a representative result of a heat map of Jaccard Indices is shown for SkBr3 breast cancer cells. 200 heterochromatin associated γH2AX clusters and 200 non-heterochromatin associated γH2AX clusters were selected by determining those with the highest and lowest heterochromatic densities in the environment and examined according to

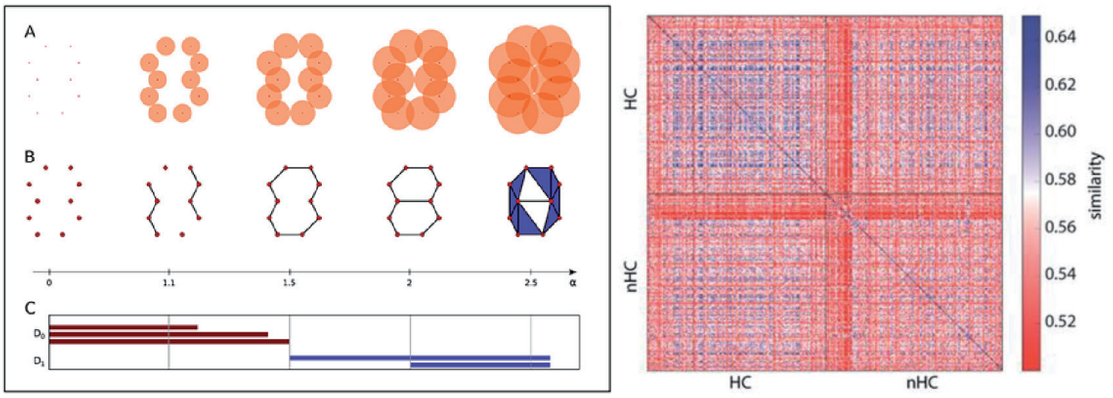

Figure 8.
Left: Illustration of the barcode data representation. (A) Continuously growing spheres, exemplarily depicted at 5 different scales α, around the point data illustrate the idea of the α-shape filtration. (B) As the growing spheres mutually embed the Centre of each-other the corresponding centres are connected by an edge. Whenever a triangle is formed, it is included in the complex as a face element. (C) Barcodes (Betti numbers) of dimension 0 (D_0) and 1 (D_1) corresponding to connected components and holes. Right: Heat map depicting the Jaccard indices averaged from components and holes for similarity of (non-)heterochromatin associated γH2AX clusters. Note: These figures are modified and were originally published under CC BY license in [138].

their topological similarity. For the average similarity for components and holes, heterochromatin associated γH2AX clusters showed a clear similarity whereas non-heterochromatin associated γH2AX clusters did not. This means that by topological analysis the heterochromatin associated γH2AX clusters could be discriminated as those clusters of high topological similarity [138]. The proximity of γH2AX clusters to heterochromatin seems to have a significant measurable impact on its structure. Interestingly, the non-heterochromatin associated γH2AX clusters and heterochromatin associated γH2AX clusters were more similar than the non-heterochromatin associated γH2AX clusters themselves. It can be clearly seen that the proximity to heterochromatin influences the structure of the clusters.

For particle irradiated NHDF cells and U87 cells, the similarity values obtained by averaging of components and holes values for each 53BP1 cluster were determined and the clusters of the 10° irradiations scheme were compared. The Jaccard indices revealed values between 0.55 and 0.82 for U87 and NHDF cells. The broad frequency distribution did not show a peak for NHDF cells whereas for U87 cells a clear peak at 0.64 was found. If the clusters of the 90° irradiation scheme were compared, the peak was located at 0.63 for U87 cells. This value was the same, if the 10° with the 90° irradiation scheme was compared. For these two comparisons (90° vs. 90°, 10° vs. 90°), NHDF cells revealed a bimodal peak distribution where one peak was located at 0.67 and the other one at 0.72 (**Figure 9**). Thus, it can be concluded that in case of the more radio-sensitive NHDF cells a higher topological similarity in 53BP1 clustering was identified than the case the less radio-sensitive U87 cells.

5.3.4 Retrotransposon Alu dosimetry

Alu short interspersed elements (SINEs) make up 11% of the human genome with over 1 million copies [150]; thereby making them ideal markers for assessing global chromatin architecture and dynamics by SMLM. Despite their involvement in many diseases of modern human [151–158] and post-transcriptional regulation [159–166], evidence grows that Alu elements are significantly regulating genome integrity and stability as a response to environmental stress. Concordantly, RNA Pol III transcriptional activation of Alu elements upon chemically and radiation induced DNA damage was observed [167] and epigenetic changes, such as DNA

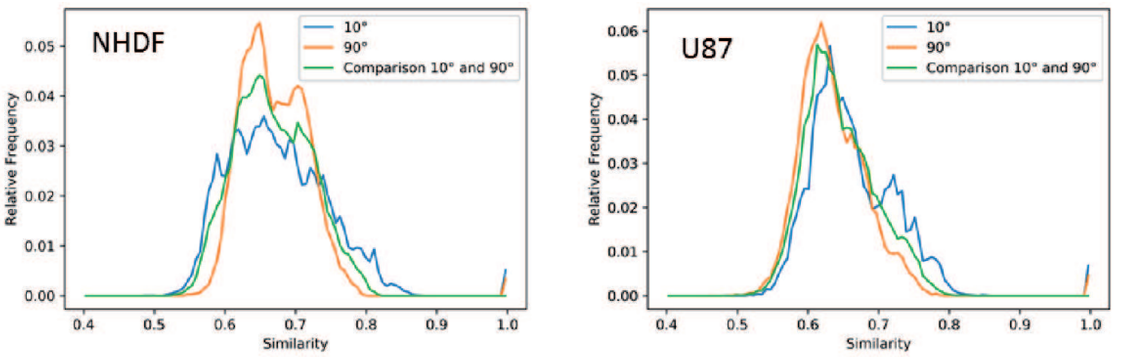

Figure 9.
"Normalized histograms of the frequencies of similarity values of barcodes (Jaccard indices) of 53BP1 clusters in NHDF and U87 cells irradiated under 10° or 90° irradiation angle and fixed 2h post irradiation. The distributions of the average similarity of dimension 0 and 1 barcodes of 53BP1 clusters in NHDF and U87 cells are shown. The similarity distributions of clusters in cells irradiated under an angle of 10° are shown in blue, the similarity distributions of clusters in cells irradiated under 90° are shown in orange, and the similarity distributions obtained when comparing clusters in cells irradiated with 10° to clusters in cells irradiated with 90° are depicted in green". Note: These figures are modified and were originally published together with the cited figure legend under CC BY license in [147].

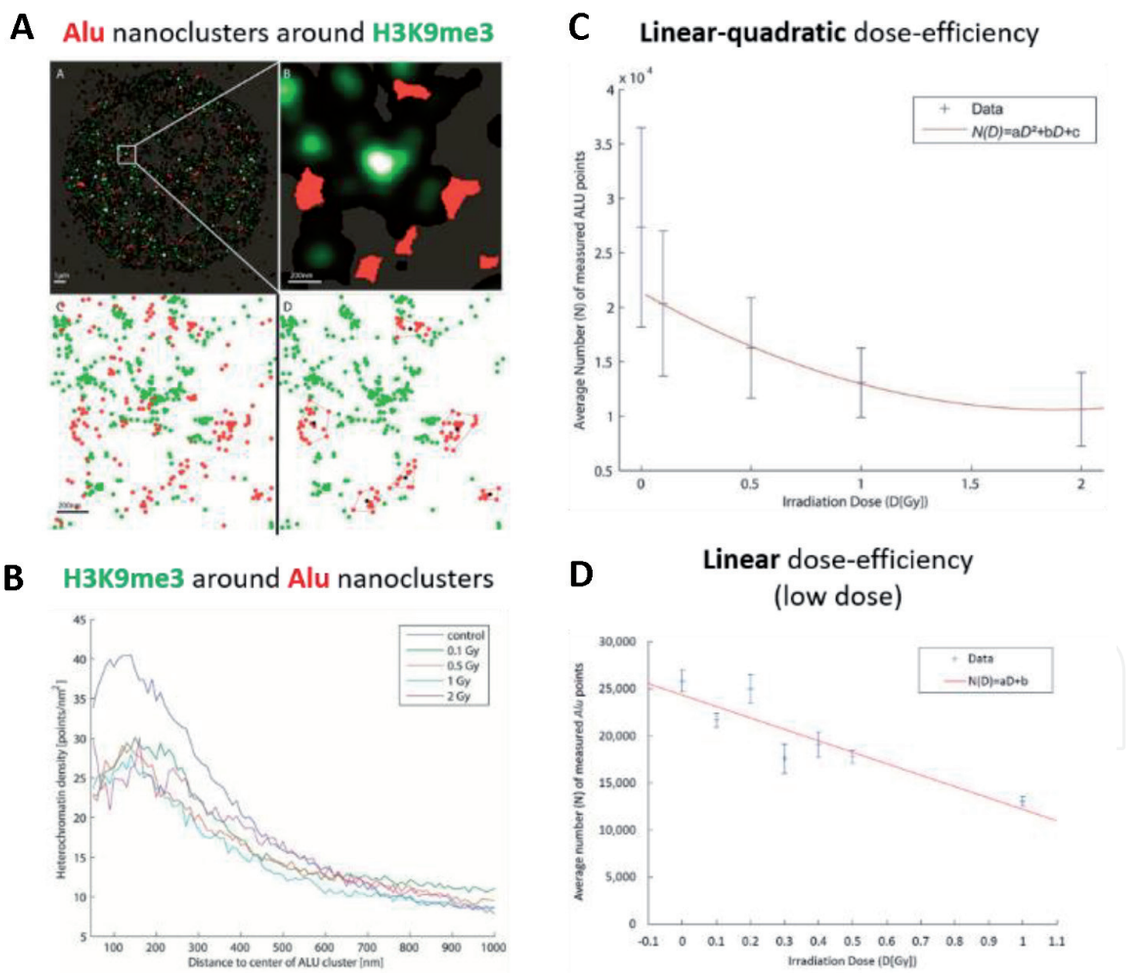

Figure 10.
(A) Single molecule localization microscopy analysis of Alu clustering and dose dependent effects of numbers of Alu labelling points after exposure to ionizing photon radiation. (B) Density distribution of heterochromatin labelling in concentric rings around the center of ALU clusters. The reduction of the density peak corresponding to heterochromatin relaxation around the Alu clusters was independent of the dose. (C) Linear quadratic dose response observed by SMLM of specific oligonucleotide nanoprobe labeling of Alu elements in SkBr3 cells after exposure to different doses of γ-radiation. (D) Linear dose response observed by SMLM of specific oligonucleotide nanoprobe labeling of Alu elements in SkBr3 cells after exposure to low doses of γ-radiation. Note: These figures are modified and were originally published under CC BY license in [16, 167].

hypomethylation, in Alu elements are differently induced in human cell lines, when exposed to different types of radiation [168].

SMLM of irradiated breast cancer cells stained by combinatorial fluorescence in situ hybridization (COMBO-FISH) [169, 170] with a unique, short 17-mer oligonucleotide specific for genomic Alu elements (**Figure 10A**) resulted in a negative linear quadratic decline of the dose efficiency curve of localization signal points in the 0.5 Gy to 4 Gy dose range (**Figure 10C**) [170]. Furthermore, differential association of Alu signals with H3K9me3 heterochromatin between irradiated and non-irradiated cells could be revealed (**Figure 10B**). The heterochromatin relaxed after irradiation. However, the extension of this relaxation was independent of the dose. Alu dosimetry was also applied to the low dose range (< 0.5 Gy) (**Figure 10D**) [16], thereby opening new paths to study the molecular mechanisms underlying the controversial low dose radiation effects [171–175], which are difficult to assess due to a lack of appropriate biomarkers for the <0.5 Gy dose range [176].

6. Conclusion and perspectives

With this article, we have addressed scientists, researchers, and clinicians working in interdisciplinary fields, which are searching for a brief introduction to current radiobiology, its fundamental principles and methodologies. We would further like to have caught the attention of radiation biologists in laboratories, clinics, and industry by demonstrating novel super-resolution microscopy techniques that have the potential to drive radiobiology to a next generation. Single molecule localization allows geometrical and topological analyses on the meso- and nano-scale at the single-cell level in situ with the advantages of easy practice and the applicability to already existing experimental methods (e.g. immunostaining, FISH). As super-resolution microscopy techniques are still not a wide-spread routine in molecular biology laboratories, the long history of fluorescence microscopy data from radiobiological studies provides a solid basis for validation. We have shown that radiobiology can be an application of SMLM based nanoscopy and its versatile data analysis method which allow the investigation of new perspectives of DNA damage induction and repair. It can even help to discover novel markers of biological dosimetry as demonstrated by our recent studies assessing dose dependent effects on retrotransposon Alu availability. Nano-scaled analysis of repair foci architecture and dynamics by assessing foci like 53BP1, Mre11, etc. will give further insight into the molecular mechanisms of DNA damage response and fate of repair pathway of individual damage sites in single cells. Indeed, evidence grows that nanostructure and function of chromatin are highly interdependent aspects that govern the fundamentals of molecular genetics, such as cell type differentiation, gene expression, DNA damage repair and reproduction. Thus, super-resolution radiobiology could serve as a general proof of principle for many other molecular biology applications in future. Finally, we believe that single-molecule localization microscopy will develop to a standard application of radiation biology and might even add to the repertoire of diagnostic technologies in clinical facilities in the future.

Acknowledgements

The successful collaborations with Felix Bestvater, German Cancer Research Center (DKFZ), Heidelberg, Christoph Cremer, Institute for Pharmacy and Molecular Biotechnology, Heidelberg University, Dieter W. Heermann, Institute

for Theoretical Physics, Heidelberg University, Harry Scherthan, Institute for Radiobiology of the Bundeswehr, Munich, and Martin Falk, Institute of Biophysics, Czech Academy of Sciences, Brno, are gratefully acknowledged. The work was supported by the project grant ("Einflüsse strahleninduzierter, multipler und einzelner spezifisch-targetierter DNA-Strangschäden auf die übergeordnete meso- und nanoskalige Chromatinarchitektur und die Topologie von Reparaturfoci" (NANOSTRANG)) of the Federal Ministry of Education and Research.

Conflict of interest

There is no conflict of interest for any of the authors.

Author details

Jin-Ho Lee[1,2] and Michael Hausmann[1*]

1 Kirchhoff-Institute for Physics, Heidelberg University, Heidelberg, Germany

2 Radiation Biology Unit (S-US), Department of Safety and Radiation Protection, FZ Jülich GmbH, Juelich, Germany

*Address all correspondence to: hausmann@kip.uni-heidelberg.de

References

[1] Falk M, Hausmann M, Lukášová E,Biswas A, Hildenbrand G, Davídková M, Krasavin E, Kleibl Z, Falková I, Ježková L, Štefančíková L, Ševčík J, Hofer M, Bačíková A, Matula P, Boreyko A, Vachelová J, Michaelidisová A, Kozubek S (2014) Determining OMICS spatiotemporal dimensions using exciting new nanoscopy techniques to asses complex cell responses to DNA damage – PART A (Radiomics). Crit. Rev. Eukaryot. Gene Express. 24: 205-223

[2] Falk M, Hausmann M, Lukášová E, Biswas A, Hildenbrand G, Davídková M, Krasavin E, Kleibl Z, Falková I, Ježková L, Štefančíková L, Ševčík J, Hofer M, Bačíková A, Matula P, Boreyko A, Vachelová J, Michaelidisová A, Kozubek S (2014) Determining OMICS spatiotemporal dimensions using exciting new nanoscopy techniques to asses complex cell responses to DNA damage – PART B (Structuromics). Crit. Rev. Eukaryot. Gene Express. 24: 225-247

[3] Bolus NE (2001). Basic review of radiation biology and terminology. J. Nucl. Med. Technol. 29: 67-73; test 76-67

[4] Martin CJ, Sutton DG, editors. Practical Radiation Protection in Healthcare. 2nd edit. Oxford University Press; 2015.DOI: 10.1093/med/9780199655212.001.0001

[5] Falk M, Hausmann M (2021) A paradigm revolution or just better resolution – will newly emerging super-resolution techniques recognize chromatin architecture as a key factor in radiation DNA damaging and repair regulation? Cancers, 13, 18. https://dx.doi.org/10.3390/cancers13010018

[6] Cremer C, Masters BR (2013) Resolution enhancement techniques in microscopy. Eur Phys J H 38: 281-344.

[7] Cremer C, Kaufmann R, Gunkel M, Pres S, Weiland Y, Müller P, Ruckelshausen T, Lemmer P, Geiger F, Degenhard M, Wege C, Lemmermann N, Holtappels R, Strickfaden H, Hausmann M (2011) Superresolution imaging of biological nanostructures by Spectral Precision Distance Microscopy (SPDM). Review. Biotech. J. 6: 1037-1051

[8] Reid DA, Rothenberg E (2015) Single-molecule fluorescence imaging techniques. Encyclopedia Anal Chem. doi:10.1002/9780470027318.a9494

[9] Thompson RE, Larson DR, Webb WW (2002) Precise nanometer localization analysis for individual fluorescent probes. Biophys J 82: 2775-2783

[10] Hendrix J, Flors C, Dedecker P, Hofkens J, Engelborghs Y (2008) Dark states in monomeric red fluorescent proteins studied by fluorescence correlation and single molecule spectroscopy. Biophysical Journal 94: 4103-4113

[11] Sinnecker D, Voigt P, Hellwig N, Schaefer M (2005) Reversible photobleaching of enhanced green fluorescent proteins. Biochemistry 44: 7085-7094

[12] Betzig E, Patterson GH, Sougrat R, Lindwasser OW, Olenych S, Bonifacino J, Davidson MW, Lippincott-Schwartz J, Hess HF (2006) Imaging intracellular fluorescent proteins at nanometer resolution. Science 313: 1642-1645

[13] Hess ST, Girirajan TP, Mason MD (2006) Ultra-high resolution imaging by fluorescence photoactivation localization microscopy. Biophys J 91: 4258-4272

[14] Lemmer P, Gunkel M, Baddeley D, Kaufmann R, Urich A,

Weiland Y, Reymann J, Müller P, Hausmann M, Cremer C (2008) SPDM – light microscopy with single molecule resolution at the nanoscale. Appl. Phys. B 93: 1-12

[15] Rust MJ, Bates M, Zhuang X (2006) Sub-diffraction-limit imaging by stochastic optical reconstruction microscopy (STORM). Nat Methods 3: 793-796

[16] Hausmann M, Ilić N, Pilarczyk G, Lee J-H, Logeswaran A, Borroni AP, Krufczik M, Theda F, Waltrich N, Bestvater F, Hildenbrand G, Cremer C, Blank M (2017) Challenges for super-resolution localization microscopy and biomolecular fluorescent nano-probing in cancer research. Int J Mol Sci 18: 2066; doi:10.3390/ijms18102066

[17] Lemmer P, Gunkel M, Weiland Y, Müller P, Baddeley D, Kaufmann R, Urich A, Eipel H, Amberger R, Hausmann M, Cremer C (2009) Using conventional fluorescent markers for far-field fluorescence localization nanoscopy allows resolution in the 10 nm range. J Microsc 235: 163-171

[18] Bohn M, Diesinger P, Kaufmann R, Weiland Y, Müller P, Gunkel M, von Ketteler A, Lemmer P, Hausmann M, Heermann DW, Cremer C (2010) Localization microscopy reveals expression-dependent parameters of chromatin nanostructure. Biophys J 99: 1358-1367

[19] Boyd PS, Struve N, Bach M, Eberle JP, Gote M, Schock F, Cremer C, Kriegs M, Hausmann M (2016) Clustered localization of EGFRvIII in glioblastoma cells as detected by high precision localization microscopy. Nanoscale 8: 20037-20047

[20] Pilarczyk G., Papenfuß F, Bestvater F, Hausmann M (2019) Spatial arrangements of Connexin43 in cancer related cells and re-arrangements under treatment conditions: Investigations on the nano-scale by super-resolution localization light microscopy. Cancers 11: 301. doi:10.3390/cancers1103030

[21] Pilarczyk G, Nesnidal I, Gunkel M, Bach M, Bestvater F, Hausmann M (2017) Localisation microscopy of breast epithelial ErbB-2 receptors and gap junctions: Trafficking after gamma-irradiation, Neuregulin-1b and Herceptin application. Int J Mol Sci 18: 362; doi:10.3390/ijms18020362

[22] Bartosova M, Herzog R, Ridinger D, Levai E, Jenei H, Zhang C, González Mateo GT, Marinovic I, Hackert T, Bestvater F, Hausmann M, López Cabrera M, Kratochwill K, Zarogiannis SG, Schmitt CP (2020) Alanyl-glutamine restores tight junction organization after disruption by a conventional peritoneal dialysis fluid. Biomolecules 10: 1178; doi: 10.3390/biom10081178

[23] Stuhlmüller M, Schwarz-Finsterle J, Fey E, Lux J, Bach M, Cremer C, Hinderhofer K, Hausmann M, Hildenbrand G (2015) In situ optical sequencing and nano-structure analysis of a trinucleotide expansion region by localization microscopy after specific COMBO-FISH labelling. Nanoscale 7: 17938-17946

[24] Eberle JP, Rapp A, Krufczik M, Eryilmaz M, Gunkel M, Erfle H, Hausmann M (2017) Super-resolution microscopy techniques and their potential for applications in radiation biophysics. In: Erfle H, editor. Super-resolution Microscopy – Methods and Protocols. Meth Molec Biol 1663: 1-13

[25] Mladenov E, Iliakis G (2011). Induction and repair of DNA double strand breaks: the increasing spectrum of non-homologous end joining pathways. Mutat Res 711, 61-72

[26] Iliakis G, Mladenov E, Mladenova V (2019) Necessities in the processing of DNA double strand breaks and their effects on genomic instability and

cancer. Cancers 11: 1671, doi:10.3390/cancers11111671

[27] Podgorsak EB (2005) Basic radiation physics. In: Podgorsak EB, editor. Radiation oncology physics : a handbook for teachers and students. IAEA, Vienna: pp 1-44

[28] Seuntjens JP, Strydom W, Shortt KR (2005) Dosimetric principles, quantities and units. In: Podgorsak EB, editor. Radiation oncology physics : a handbook for teachers and students. IAEA, Vienna: pp 45-70

[29] Podgorsak EB, Podgorsak MB (2005) Special procedures and techniques in radiotherapy. In: Podgorsak EB, editor. Radiation oncology physics : a handbook for teachers and students. IAEA, Vienna: pp 505-548

[30] Durante M, Orecchia R, Loeffler JS (2017) Charged-particle therapy in cancer: Clinical uses and future perspectives. Nat Rev Clin Oncol 14: 483-495

[31] Ortiz López P, Rajan G, Podgorsak EB (2005) Radiation protection and safety in radiotherapy. In: Podgorsak EB, editor. Radiation oncology physics : a handbook for teachers and students. IAEA, Vienna: pp 549-638

[32] Reisz JA, Bansal N, Qian J, Zhao W, Furdui CM (2014). Effects of ionizing radiation on biological molecules--mechanisms of damage and emerging methods of detection. Antioxid Redox Signal 21: 260-292

[33] Jeggo PA, Pearl LH, Carr AM (2016) DNA repair, genome stability and cancer: a historical perspective. Nat Rev Cancer 16: 35-42, doi:10.1038/nrc.2015.4

[34] Ward JF (1990). The yield of DNA double-strand breaks produced intracellularly by ionizing radiation: a review. Int J Radiat Biol 57: 1141-1150

[35] Mladenov E, Magin S, Soni A, Iliakis G (2013). DNA double-strand break repair as determinant of cellular radiosensitivity to killing and target in radiation therapy. Front Oncol 3: 113

[36] Iliakis G (1991). The role of DNA double strand breaks in ionizing radiation-induced killing of eukaryotic cells. Bioessays 13: 641-648

[37] Povirk LF (2006). Biochemical mechanisms of chromosomal translocations resulting from DNA double-strand breaks. DNA Repair (Amst) 5: 1199-1212

[38] Rogakou EP, Pilch DR, Orr AH, Ivanova VS, Bonner WM (1998) DNA double-stranded breaks induce histone H2AX phosphorylation on serine 139. J Biol Chem 273: 5858-5868

[39] Rogakou EP, Boon C, Redon C, Bonner WM (1999) Megabase chromatin domains involved in DNA double-strand breaks in vivo. J Cell Biol 146: 905-916

[40] Redon CE, Dickey JS, Bonner WM, Sedelnikova OA (2009) γ-H2AX as a biomarker of DNA damage induced by ionizing radiation in human peripheral blood lymphocytes and artificial skin. Adv Space Res 43: 1171-1178, doi:10.1016/j.asr.2008.10.011

[41] Kinner A, Wu W, Staudt C, Iliakis G (2008). γ-H2AX in recognition and signaling of DNA double-strand breaks in the context of chromatin. Nucleic Acids Res 36: 5678-5694

[42] Jezkova L, Zadneprianetc M, Kulikova E, Smirnova E, Bulanova T, Depes D, Falkova I, Boreyko A, Krasavin E, Davidkova M, Kozubek S, Valentova O, Falk M (2018) Particles with similar LET values generate DNA breaks of different complexity and reparability: a high-resolution microscopy analysis of γH2AX/53BP1 foci. Nanoscale 10: 1162-1179, doi:10.1039/c7nr06829h.

[43] Desouky O, Ding N, Zhou G (2015). Targeted and non-targeted effects of ionizing radiation. J Radiat Res Appl Sci 8: 247-254

[44] Srinivas US, Tan BWQ, Vellayappan BA, Jeyasekharan AD (2019) ROS and the DNA damage response in cancer. Redox Biology 25: 101084, doi.org/10.1016/j.redox.2018.101084

[45] Ward JF (2000). Complexity of damage produced by ionizing radiation. Cold Spring Harb Symp Quant Biol 65: 377-382

[46] Zhao L, Bao C, Shang Y, He X, Ma C, Lei X, Mi D, Sun Y (2020) The determinant of DNA repair pathway choices in ionizing radiation-induced DNA double-strand breaks. BioMed Res Int 2020: 1-12, doi:10.1155/2020/4834965

[47] Shibata A (2017) Regulation of repair pathway choice at two-ended DNA double-strand breaks. Mutat Res: 803-805, 51-55, doi:10.1016/j.mrfmmm.2017.07.011.

[48] Clouaire T, Legube G (2015) DNA double strand break repair pathway choice: a chromatin based decision? Nucleus 6: 107-113, doi:10.1080/19491034.2015.1010946

[49] Goldstein, M., and Kastan, M.B. (2015). The DNA damage response: implications for tumor responses to radiation and chemotherapy. Annu Rev Med 66, 129-143

[50] Ensminger M, Löbrich M (2020) One end to rule them all: Non-homologous end-joining and homologous recombination at DNA double-strand breaks. Brit J Radiol: 20191054, doi:10.1259/bjr.20191054

[51] Xiong X, Du Z, Wang Y, Feng Z, Fan P, Yan C, Willers H, Zhang J (2015) 53BP1 promotes microhomology-mediated end-joining in G1-phase cells. Nucl Acids Res 43: 1659-1670, doi:10.1093/nar/gku1406

[52] Mladenov E, Magin S, Soni A, Iliakis G (2016) DNA double-strand-break repair in higher eukaryotes and its role in genomic instability and cancer: Cell cycle and proliferation-dependent regulation. Semin Cancer Biol: 37-38, 51-64, doi:10.1016/j.semcancer.2016.03.003

[53] Arnould C, Legube G (2020) The secret life of chromosome loops upon DNA double-strand break. J Mol Biol 432: 724-736

[54] Cromie GA, Connelly JC, Leach DR (2001). Recombination at double-strand breaks and DNA ends: conserved mechanisms from phage to humans. Mol Cell 8, 1163-1174

[55] Sallmyr A, Tomkinson AE (2018) Repair of DNA double-strand breaks by mammalian alternative end-joining pathways. J Biol Chem 293: 10536-10546, doi:10.1074/jbc.TM117.000375

[56] Chang HHY, Pannunzio NR, Adachi N, Lieber MR (2017) Non-homologous DNA end joining and alternative pathways to double-strand break repair. Nat Rev Mol Cell Biol 18: 495-506, doi:10.1038/nrm.2017.48

[57] Iliakis G, Murmann T, Soni A (2015) Alternative end-joining repair pathways are the ultimate backup for abrogated classical non-homologous end-joining and homologous recombination repair: Implications for the formation of chromosome translocations. Mutat Res Genet Toxicol Environ Mutagen 793: 166-175, doi:10.1016/j.mrgentox.2015.07.001.

[58] Iliakis G (2009) Backup pathways of NHEJ in cells of higher eukaryotes: cell cycle dependence. Radiother Oncol 92: 310-315, doi:10.1016/j.radonc.2009.06.024

[59] Verma P, Greenberg RA (2016) Noncanonical views of homology-directed DNA repair. Genes Development 30: 1138-1154, doi:10.1101/gad.280545.116

[60] Bunting SF, Callen E, Wong N, Chen HT, Polato F, Gunn A, Bothmer A, Feldhahn N, Fernandez-Capetillo O, Cao L, et al. (2010) 53BP1 inhibits homologous recombination in Brca1-deficient cells by blocking resection of DNA breaks. Cell 141: 243-254

[61] Chang HHY, Pannunzio NR, Adachi N, Lieber MR (2017). Non-homologous DNA end joining and alternative pathways to double-strand break repair. Nat Rev Mol Cell Biol 18: 495-506

[62] Escribano-Diaz C, Orthwein A, Fradet-Turcotte A, Xing M, Young JT, Tkac J, Cook MA, Rosebrock AP, Munro M, Canny MD, et al. (2013) A cell cycle-dependent regulatory circuit composed of 53BP1-RIF1 and BRCA1-CtIP controls DNA repair pathway choice. Mol Cell 49: 872-883

[63] Lieber MR (2010). The mechanism of double-strand DNA break repair by the nonhomologous DNA end-joining pathway. Annu Rev Biochem 79: 181-211

[64] Yano K., Chen DJ (2008) Live cell imaging of XLF and XRCC4 reveals a novel view of protein assembly in the non-homologous end-joining pathway. Cell Cycle 7: 1321-1325

[65] Gottlieb TM, Jackson SP (1993) The DNA-dependent protein kinase: requirement for DNA ends and association with Ku antigen. Cell 72: 131-142

[66] Meek K, Dang V, Lees-Miller SP (2008) DNA-PK: the means to justify the ends? Adv Immunol 99: 33-58

[67] Goodarzi AA, Yu Y, Riballo E, Douglas P, Walker SA, Ye R, Harer C, Marchetti C, Morrice N, Jeggo PA, et al. (2006). DNA-PK autophosphorylation facilitates Artemis endonuclease activity. EMBO J 25: 3880-3889

[68] Cui X, Yu Y, Gupta S, Cho YM, Lees-Miller SP, Meek K (2005) Autophosphorylation of DNA-dependent protein kinase regulates DNA end processing and may also alter double-strand break repair pathway choice. Mol Cell Biol 25: 10842-10852

[69] Cottarel J, Frit P, Bombarde O, Salles B, Negrel A, Bernard S, Jeggo PA, Lieber MR, Modesti M, Calsou P (2013). A noncatalytic function of the ligation complex during nonhomologous end joining. J Cell Biol 200: 173-186

[70] Gu J, Lu H, Tippin B, Shimazaki N, Goodman MF, Lieber MR (2007) XRCC4: DNA ligase IV can ligate incompatible DNA ends and can ligate across gaps. EMBO J 26: 1010-1023

[71] Tsai CJ, Kim SA, Chu G (2007). Cernunnos/XLF promotes the ligation of mismatched and noncohesive DNA ends. Proc Natl Acad Sci U S A 104: 7851-7856

[72] Kurosawa A, Koyama H, Takayama S, Miki K, Ayusawa D, Fujii M, Iiizumi S, Adachi N (2008) The requirement of Artemis in double-strand break repair depends on the type of DNA damage. DNA Cell Biol 27: 55-61

[73] Riballo E, Kuhne M, Rief N, Doherty A, Smith GC, Recio MJ, Reis C, Dahm K, Fricke A, Krempler A, et al. (2004) A pathway of double-strand break rejoining dependent upon ATM, Artemis, and proteins locating to gamma-H2AX foci. Mol Cell 16: 715-724

[74] Chappell C, Hanakahi LA, Karimi-Busheri F, Weinfeld M, West SC (2002) Involvement of human polynucleotide kinase in double-strand

break repair by non-homologous end joining. EMBO J 21: 2827-2832

[75] Vignard J, Mirey G, Salles B (2013) Ionizing-radiation induced DNA double-strand breaks: a direct and indirect lighting up. Radiother Oncol 108: 362-369

[76] Lamarche BJ, Orazio NI, Weitzman MD (2010) The MRN complex in double-strand break repair and telomere maintenance. FEBS Lett 584: 3682-3695

[77] Shiloh Y, Ziv Y (2013) The ATM protein kinase: regulating the cellular response to genotoxic stress, and more. Nat Rev Mol Cell Biol 14: 197-210

[78] Uziel T, Lerenthal Y, Moyal L, Andegeko Y, Mittelman L, Shiloh Y (2003) Requirement of the MRN complex for ATM activation by DNA damage. EMBO J 22: 5612-5621

[79] Paull TT (2015) Mechanisms of ATM Activation. Annu Rev Biochem 84: 711-738

[80] Makharashvili N, Paull TT (2015) CtIP: A DNA damage response protein at the intersection of DNA metabolism. DNA Repair (Amst) 32: 75-81

[81] Eid W, Steger M, El-Shemerly M, Ferretti LP, Pena-Diaz J, Konig C, Valtorta E, Sartori AA, Ferrari S (2010) DNA end resection by CtIP and exonuclease 1 prevents genomic instability. EMBO Rep 11: 962-968

[82] Cannavo E, Cejka P, Kowalczykowski SC (2013) Relationship of DNA degradation by *Saccharomyces cerevisiae* exonuclease 1 and its stimulation by RPA and Mre11-Rad50-Xrs2 to DNA end resection. Proc Natl Acad Sci USA 110: E1661-1668

[83] Cejka P (2015) DNA end resection: Nucleases team up with the right partners to initiate homologous recombination. J Biol Chem 290: 22931-22938

[84] Tsutakawa SE, Lafrance-Vanasse J, Tainer JA (2014) The cutting edges in DNA repair, licensing, and fidelity: DNA and RNA repair nucleases sculpt DNA to measure twice, cut once. DNA Repair (Amst) 19: 95-107

[85] Kim DH, Lee KH, Kim JH, Ryu GH, Bae SH, Lee BC, Moon KY, Byun SM, Koo HS, Seo YS (2005) Enzymatic properties of the *Caenorhabditis elegans* Dna2 endonuclease/helicase and a species-specific interaction between RPA and Dna2. Nucleic Acids Res 33: 1372-1383

[86] Baumann P, West SC (1998) Role of the human RAD51 protein in homologous recombination and double-stranded-break repair. Trends Biochem Sci 23: 247-251

[87] Bugreev DV, Hanaoka F, Mazin AV (2007) Rad54 dissociates homologous recombination intermediates by branch migration. Nat Struct Mol Biol 14: 746-753

[88] Mazin AV, Mazina OM, Bugreev DV, Rossi MJ (2010) Rad54, the motor of homologous recombination. DNA Repair (Amst) 9: 286-302

[89] Haince JF, McDonald D, Rodrigue A, Dery U, Masson JY, Hendzel MJ, Poirier GG (2008) PARP1-dependent kinetics of recruitment of MRE11 and NBS1 proteins to multiple DNA damage sites. J Biol Chem 283: 1197-1208

[90] Arakawa H, Bednar T, Wang M, Pau, K, Mladenov E, Bencsik-Theilen AA, Iliakis G (2012) Functional redundancy between DNA ligases I and III in DNA replication in vertebrate cells. Nucleic Acids Res 40: 2599-2610

[91] Paul K, Wang M, Mladenov E, Bencsik-Theilen A, Bednar T, Wu W,

Arakawa H, Iliakis G (2013) DNA ligases I and III cooperate in alternative non-homologous end-joining in vertebrates. PLoS One 8: e59505

[92] Symington LS (2016) Mechanism and regulation of DNA end resection in eukaryotes. Crit Rev Biochem Mol Biol 51: 195-212

[93] Symington LS (2002) Role of RAD52 epistasis group genes in homologous recombination and double-strand break repair. Microbiol Mol Biol Rev 66: 630-670

[94] Elliott B, Richardson C, Jasin M (2005) Chromosomal translocation mechanisms at intronic alu elements in mammalian cells. Mol Cell 17: 885-894

[95] Weinstock DM, Elliott B, Jasin M (2006) A model of oncogenic rearrangements: differences between chromosomal translocation mechanisms and simple double-strand break repair. Blood 107: 777-780

[96] Morales ME, White TB, Streva VA, DeFreece CB, Hedges DJ, Deininger PL (2015) The contribution of alu elements to mutagenic DNA double-strand break repair. PLoS Genet 11: e1005016

[97] Fowler JF (2010) 21 years of biologically effective dose. Br J Radiol 83: 554-568

[98] McMahon SJ, Schuemann J, Paganetti H, Prise KM (2016) Mechanistic Modelling of DNA Repair and Cellular Survival Following Radiation-Induced DNA Damage. Scientific Reports 6: 33290

[99] Falk M, Wolinsky M, Veldwijk MR, Hildenbrand G, Hausmann M (2020) Gold nanoparticle enhanced radiosensitivity of cells: Considerations and contradictions from model systems and basic investigations of cell damaging for radiation therapy. In: Sajo E, Zygmanski P, editors, Nanoparticle Enhanced Radiation Therapy – Principles, Methods and Applications, IOP Publishing Ltd 2020, pp. 10-1 – 10-25, doi. org/10.1088/978-0-7503-2396-3ch10

[100] Puck TT, Marcus PI (1956) Action of x-rays on mammalian cells. J Exp Med 103: 653-666

[101] Wang Q, Sun Z, Du L, Xu C, Wang Y, Yang B, He N, Wang J, Ji K, Liu Y, Liu Q (2018) Melatonin sensitizes human colorectal cancer cells to X-ray ionizing radiation in vitro and in vivo. Int J Mol Sci 19: 3974, doi:10.3390/ijms19123974

[102] Yoshikawa H, Sunada S, Hirakawa H, Fujimori A, Elmegerhi S, Leary D, Kato TA (2019) Radiobiological characterization of canine malignant melanoma cell lines with different types of ionizing radiation and efficacy evaluation with cytotoxic agents. Int J Mol Sci 20; 841, doi:10.3390/ijms20040841

[103] Suntharalingam N, Podgorsak EB, Hendry JH (2005) Basic radiobiology. In: Podgorsak EB, editor. Radiation oncology physics : a handbook for teachers and students. IAEA, Vienna: pp 485-504

[104] Agrawala PK, Adhikari JS, Chaudhury NK (2010) Lymphocyte chromosomal aberration assay in radiation biodosimetry. J Pharm Bioallied Sci 2: 197-201

[105] Bender MA, Gooch PC (1962) Types and rates of x-ray-induced chromosome aberrations in human blood irradiated in vitro. Proc Natl Acad Sci U S A 48: 522-532

[106] Blakely WF, Carr Z, Chu MC, Dayal-Drager R, Fujimoto K, Hopmeir M, Kulka U, Lillis-Hearne P, Livingston GK, Lloyd DC, et al. (2009) WHO 1st consultation on the development of a global biodosimetry

laboratories network for radiation emergencies (BioDoseNet). Radiat Res 171: 127-139

[107] Schmid W (1975) The micronucleus test. Mutat Res 31: 9-15

[108] Doherty AT (2012) The in vitro micronucleus assay. Methods Mol Biol 817: 121-141

[109] Ostling O, Johanson KJ (1984) Microelectrophoretic study of radiation-induced DNA damages in individual mammalian cells. Biochem Biophys Res Commun 123: 291-298

[110] Singh NP, McCoy MT, Tice RR, Schneider EL (1988) A simple technique for quantitation of low levels of DNA damage in individual cells. Exp Cell Res 175: 184-191

[111] Collins AR (2004) The comet assay for DNA damage and repair: principles, applications, and limitations. Mol Biotechnol 26: 249-261

[112] Albert O, Reintsch WE, Chan P, Robaire, B (2016) HT-COMET: a novel automated approach for high throughput assessment of human sperm chromatin quality. Hum Reprod 31: 938-946

[113] Ge J, Chow DN, Fessler JL, Weingeist DM, Wood DK, Engelward BP (2015) Micropatterned comet assay enables high throughput and sensitive DNA damage quantification. Mutagenesis 30: 11-19

[114] Lee T, Lee S, Sim WY, Jung YM, Han S, Won JH, Min H, Yoon S (2018) HiComet: a high-throughput comet analysis tool for large-scale DNA damage assessment. BMC Bioinformatics 19: 44

[115] Cremer C, Masters BR (2013) Resolution enhancement techniques in microscopy. Eur Phys J H 38: 281-344

[116] Nahidiazar L, Agronskaia AV, Broertjes J, van den Broek B, Jalink K (2016) Optimizing imaging conditions for demanding multi-color super resolution localization microscopy. PLoS One 11: e0158884

[117] Kaufmann R, Lemmer P, Gunkel M, Weiland Y, Müller P, Hausmann M, Baddeley D, Amberger R, Cremer C (2009) SPDM – Single molecule superresolution of cellular nanostructures. Proc. SPIE 7185: 71850J1-71850J19

[118] Ambrose EJ (1956) A surface contact microscope for the study of cell movements. Nature 178: 1194

[119] Axelrod D (2001) Total internal reflection fluorescence microscopy in cell biology. Traffic 2: 764-774

[120] Betzig E, Lewis A, Harootunian A, Isaacson M, Kratschmer E (1986) Near Field Scanning Optical Microscopy (NSOM): Development and biophysical applications. Biophys J 49: 269-279

[121] Betzig E, Trautman JK (1992) Near-field optics: microscopy, spectroscopy, and surface modification beyond the diffraction limit. Science 257: 189-195

[122] Perner B, Rapp A, Dressler C, Wollweber L , Beuthan J, Greulich KO, Hausmann M (2002) Variations in cell surfaces of estrogen treated breast cancer cells detected by a combined instrument for far-field and near-field microscopy. Analyt Cell Pathol 24: 89-100

[123] Hausmann M, Liebe B, Perner B, Jerratsch M, Greulich KO, Scherthan H (2003) Imaging of human meiotic chromosomes by scanning near-field optical microscopy (SNOM). Micron 34: 441-447

[124] Winkler R, Perner B, Rapp A, Durm M, Cremer C, Greulich KO,

Hausmann M (2003) Labelling quality and chromosome morphology after low temperature FISH analysed by scanning far-field and scanning near-field optical microscopy. J Microsc 209: 23-33

[125] Klar TA, Hell SW (1999) Subdiffraction resolution in far-field fluorescence microscopy. Opt Lett 24: 954-956

[126] Hildenbrand G, Rapp A, Spöri U, Wagner C, Cremer C, Hausmann M (2005) Nano-sizing of specific gene domains in intact human cell nuclei by Spatially Modulated Illumination (SMI) light microscopy. Biophys J 88: 4312-4318

[127] Rauch J, Knoch TA, Solovei I, Teller K, Stein S, Buiting K, Horsthemke B, Langowski J, Cremer T, Hausmann M, Cremer C (2007/2008) Lightoptical precision measurements of the active and inactive Prader-Willi Syndrome imprinted regions in human cell nuclei. Differentiation 76: 66-82, doi:10.111/j.1432-0436.2007.00237.x]

[128] Cremer C, Edelmann P, Esa A, Bornfleth H, Schneider B, Bradl J, Rinke B, Trakhtenbrot L, Dietzel S, Hausmann M, Cremer T (1999) Spektrale Präzisionsdistanzmikroskopie in der Genomforschung. Z Med Phys 9: 14-20

[129] Esa A, Edelmann P, Kreth G, Trakhtenbrot L, Amariglio N, Rechavi G, Hausmann M, Cremer C (2000) Three-dimensional spectral precision distance microscopy of chromatin nano-structures after triple-colour DNA labelling: a study of the BCR region on chromosome 22 and the Philadelphia chromosome. J Microsc 199: 96-105

[130] Huang B, Bates M, Zhuang X (2009) Super-resolution fluorescence microscopy. Annu Rev Biochem 78: 993-1016

[131] Heilemann M, van de Linde S, Schuttpelz M, Kasper R, Seefeldt B, Mukherjee A, Tinnefeld P, Sauer M (2008) Subdiffraction-resolution fluorescence imaging with conventional fluorescent probes. Angew Chem Int Ed Engl 47: 6172-6176

[132] Folling J, Bossi M, Bock H, Medda R, Wurm CA, Hein B, Jakobs S, Eggeling C, Hell SW (2008) Fluorescence nanoscopy by ground-state depletion and single-molecule return. Nat Methods 5: 943-945

[133] Baddeley D, Jayasinghe ID, Cremer C, Cannell MB, Soeller C (2009) Light-induced dark states of organic fluochromes enable 30 nm resolution imaging in standard media. Biophys J 96: L22-24

[134] Vogel M, Gruber A, Wrachtrup J, von Borczyskowski C (1995) Determination of intersystem crossing parameters via observation of quantum jumps on single molecules. J Phys Chem 99: 14915-14917

[135] Martynski M, Zydlewicz J, Boens N, Molski A (2005) Determination of photophysical parameters from photon arrival time trajectories in single molecule fluorescence spectroscopy. J Chem Phys 122: 134507

[136] Vogelsang J, Cordes T, Forthmann C, Steinhauer C, Tinnefeld P (2009) Controlling the fluorescence of ordinary oxazine dyes for single-molecule switching and superresolution microscopy. Proc Natl Acad Sci U S A 106: 8107-8112

[137] Deschout H, Cella Zanacchi F, Mlodzianoski M, Diaspro A, Bewersdorf J, Hess ST, Braeckmans K (2014) Precisely and accurately localizing single emitters in fluorescence microscopy. Nat Methods 11: 253-66, doi: 10.1038/nmeth.2843. PMID: 24577276.

[138] Hofmann A, Krufczik M, Heermann DW, Hausmann M (2018)

Using persistent homology as a new approach for super-resolution localization microscopy data analysis and classification of γH2AX foci/clusters. Int J Mol Sci 19: 2263, doi:10.3390/ijms19082263

[139] Magenau A, Owen DM, Yamamoto Y, Tran J, Kwiatek JM, Parton RG, Gaus K (2015) Discreet and distinct clustering of five model membrane proteins revealed by single molecule localization microscopy. Mol Membr Biol 32: 11-18

[140] Hausmann M, Wagner E, Lee J-H, Schrock G, Schaufler W, Krufczik M, Papenfuß F, Port M, Bestvater F, Scherthan H (2018) Super-resolution microscopy of radiation-induced histone H2AX phosphorylation in relation to H3K9-trimethylation in HeLa cells. Nanoscale 10: 4320-4331; doi:10.1039/C7NR08145F

[141] Eryilmaz M, Schmitt E, Krufczik M, Theda F, Lee J-H, Cremer C, Bestvater F, Schaufler W, Hausmann M, Hildenbrand G (2018) Localization microscopy analyses of MRE11 clusters in 3D-conserved cell nuclei of different cell lines. Cancers 10: 25, doi:10.3390/cancers10010025

[142] Scherthan H, Lee J-H, Maus E, Schumann S, Muhtadi R, Chojowski R, Port M, Lassmann M, Bestvater F, Hausmann M (2019) Nanostructure of clustered DNA damage in leukocytes after in-solution irradiation with the alpha emitter Ra-223. Cancers 11: 1877, doi:10.3390/cancers11121877

[143] Bach M, Savini C, Krufczik M, Cremer C, Rösl F, Hausmann M (2017) Super-resolution localization microscopy of γ-H2AX and heterochromatin after folate deficiency. Int. J. Mol. Sci. 18: 1726, doi:10.3390/ijms18081726

[144] Zhang Y, Máté G, Müller P, Hillebrandt S, Krufczik M, Bach M, Kaufmann R, Hausmann M, Heermann DW (2015) Radiation induced chromatin conformation changes analysed by fluorescent localization microscopy, statistical physics, and graph theory. PLoS ONE 10: e0128555, doi:10.1371/journal.prone.0128555

[145] Depes D, Lee J-H, Bobkova E, Jezkova L, Falkova I, Bestvater F, Pagacova E, Kopecna O, Zadneprianetc M, Bacikova A, Kulikova E, Smirnova E, Bulanova T, Boreyko A, Krasavin E, Hausmann M, Falk M (2018) Single molecule localization microscopy as a promising tool for γH2AX/53BP1 foci exploration. Eur Phys J D 72: 158, doi: 10.1140/epjd/e2018-90148-1

[146] Bobkova E, Depes D, Lee J-H, Jezkova L, Falkova I, Pagacova E, Kopecna O, Zadneprianetc M, Bacikova A, Kulikova E, Smirnova E, Bulanova T, Boreyko A, Krasavin E, Wenz F, Bestvater F, Hildenbrand G, Hausmann M, Falk M (2018) Recruitment of 53BP1 proteins for DNA repair and persistence of repair clusters differ for cell types as detected by single molecule localization microscopy. Int J Molec Sci 19: 3713, doi:10.3390/ijms19123713

[147] Hausmann M, Neitzel C, Bobkova E, Nagel D, Hofmann A, Chramko T, Smirnova E, Kopečná O, Pagáčová E, Boreyko A, Krasavin E, Falkova I, Heermann DW, Pilarczyk G, Hildenbrand G, Bestvater F, Falk M (2020) Single Molecule Localization Microscopy analyses of DNA-repair foci and clusters detected along particle damage tracks. Front Phys 8: 578662, doi: 10.3389/fphy.2020.578662

[148] Máté G, Hofmann A, Wenzel N, Heermann DW (2014) A topological similarity measure for proteins. Biochim Biophys Acta BBA – Biomembr 1838: 1180-1190

[149] Jaccard P (1901) Etude comparative de la distribution florale dans une

portion des Alpes et des Jura. Bull Soc Vaud Sci Nat 37: 547-579

[150] Chae JJ, Park YB, Kim SH, Hong SS, Song GJ, Han KH, Namkoong Y, Kim HS, Lee CC (1997) Two partial deletion mutations involving the same Alu sequence within intron 8 of the LDL receptor gene in Korean patients with familial hypercholesterolemia. Hum Genet 99: 155-163

[151] Kolomietz E, Meyn MS, Pandita A, Squire JA (2002) The role of Alu repeat clusters as mediators of recurrent chromosomal aberrations in tumors. Genes Chromos Cancer 35: 97-112

[152] Lehrman MA, Goldstein JL, Russell DW, Brown MS (1987) Duplication of seven exons in LDL receptor gene caused by Alu-Alu recombination in a subject with familial hypercholesterolemia. Cell 48: 827-835

[153] Puget N, Sinilnikova OM, Stoppa-Lyonnet D, Audoynaud C, Pages S, Lynch HT, Goldgar D, Lenoir GM, Mazoyer S (1999) An Alu-mediated 6-kb duplication in the BRCA1 gene: a new founder mutation? Am J Hum Genet 64: 300-302

[154] Rohlfs EM, Puget N, Graham ML, Weber BL, Garber JE, Skrzynia C, Halperin JL, Lenoir GM, Silverman LM, Mazoyer S (2000) An Alu-mediated 7.1 kb deletion of BRCA1 exons 8 and 9 in breast and ovarian cancer families that results in alternative splicing of exon 10. Genes Chromos Cancer 28: 300-307

[155] Swensen J, Hoffman M, Skolnick MH, Neuhausen SL (1997) Identification of a 14 kb deletion involving the promoter region of BRCA1 in a breast cancer family. Hum Mol Genet 6: 1513-1517

[156] Teugels E, De Brakeleer S, Goelen G, Lissens W, Sermijn E, De Greve J (2005) De novo Alu element insertions targeted to a sequence common to the BRCA1 and BRCA2 genes. Hum Mutat 26: 284

[157] Wimmer K, Callens T, Wernstedt A, Messiaen L (2011) The NF1 gene contains hotspots for L1 endonuclease-dependent de novo insertion. PLoS Genet 7: e1002371

[158] Yamakawa K, Takada K, Yanagi H, Tsuchiya S, Kawai K, Nakagawa S, Kajiyama G, Hamaguchi H (1989) Three novel partial deletions of the low-density lipoprotein (LDL) receptor gene in familial hypercholesterolemia. Hum Genet 82, 317-321

[159] Chen C, Ara T, Gautheret D (2009) Using Alu elements as polyadenylation sites: A case of retroposon exaptation. Mol Biol Evol 26: 327-334.

[160] Chen LL, DeCerbo JN, Carmichael GG (2008) Alu element-mediated gene silencing. EMBO J 27: 1694-1705

[161] Dominissini D, Moshitch-Moshkovitz S, Amariglio N, Rechavi G (2011) Adenosine-to-inosine RNA editing meets cancer. Carcinogenesis 32: 1569-1577

[162] Levanon EY, Eisenberg E, Yelin R, Nemzer S, Hallegger M, Shemesh R, Fligelman ZY, Shoshan A, Pollock SR, Sztybel D, et al. (2004) Systematic identification of abundant A-to-I editing sites in the human transcriptome. Nat Biotechnol 22: 1001-1005

[163] Roy-Engel AM, El-Sawy M, Farooq L, Odom GL, Perepelitsa-Belancio V, Bruch H, Oyeniran OO, Deininger PL (2005) Human retroelements may introduce intragenic polyadenylation signals. Cytogenet Genome Res 110: 365-371

[164] Sela N, Mersch B, Hotz-Wagenblatt A, Ast G (2010) Characteristics of transposable element

exonization within human and mouse. PLoS One 5: e10907

[165] Shen S, Lin L, Cai JJ, Jiang P, Kenkel EJ, Stroik MR, Sato S, Davidson BL, Xing Y (2011) Widespread establishment and regulatory impact of Alu exons in human genes. Proc Natl Acad Sci U S A 108: 2837-2842

[166] Vorechovsky I (2010) Transposable elements in disease-associated cryptic exons. Hum Genet 127: 135-154

[167] Rudin CM, Thompson CB (2001) Transcriptional activation of short interspersed elements by DNA-damaging agents. Genes Chromosomes Cancer 30: 64-71

[168] Goetz W, Morgan MN, Baulch JE (2011) The effect of radiation quality on genomic DNA methylation profiles in irradiated human cell lines. Radiat Res 175: 575-587

[169] Hausmann M, Winkler R, Hildenbrand G, Finsterle J, Weisel A, Rapp A, Schmitt E, Janz S, Cremer C (2003) COMBO-FISH: specific labelling of nondenatured chromatin targets by computer-selected DNA oligonucleotide probe combinations. Biotechniques 35: 564-577

[170] Krufczik M, Sievers A, Hausmann A, Lee J-H, Hildenbrand G, Schaufler W, Hausmann M (2017) Combining low temperature fluorescence DNA-hybridization, immunostaining, and super-resolution localization microscopy for nano-structure analysis of ALU elements and their influence on chromatin structure. Int J Mol Sci 18: 1005, doi:10.3390/ijms18051005

[171] Farooque A, Mathur R, Verma A, Kaul V, Bhatt AN, Adhikari JS, Afrin F, Singh S, Dwarakanath BS (2011) Low-dose radiation therapy of cancer: role of immune enhancement. Expert Rev Anticancer Ther 11: 791-802

[172] Feinendegen LE (2005) Evidence for beneficial low level radiation effects and radiation hormesis. Br J Radiol 78: 3-7

[173] Feinendegen LE, Brooks AL, Morgan WF (2011) Biological consequences and health risks of low-level exposure to ionizing radiation: commentary on the workshop. Health Phys 100: 247-259

[174] Mathias D, Mitchel RE, Barclay M, Wyatt H, Bugden M, Priest ND, Whitman SC, Scholz M, Hildebrandt G, Kamprad M, et al. (2015) Low-dose irradiation affects expression of inflammatory markers in the heart of ApoE −/− mice. PLoS One 10: e0119661

[175] Pollycove M (1998) Nonlinearity of radiation health effects. Environ Health Perspect 106 (Suppl 1): 363-368

[176] Martin LM, Marples B, Lynch TH, Hollywood D, Marignol L (2014) Exposure to low dose ionising radiation: Molecular and clinical consequences. Cancer Lett 349: 98-106